國立臺灣大學工學院醫學工程學研究所

碩士論文

Graduate Institute of Biomedical Engineering
College of Medicine and College of Engineering
National Taiwan University

Master Thesis

動態對比增強磁共振影像參數之估測:位移效應之修正

Estimation of Dynamic Contrast Enhanced Magnetic Resonance Imaging Parameters : Motion Artifact Correction

許皓翔

Hao-Hsiang Hsu

指導教授：陳中明 博士　張允中 醫師

Advisor: Chung-Ming Chen, Ph.D.
Yeun-Chung Chang, M.D. Ph.D.

中華民國 97 年 7 月

July,2008

誌謝

首先，我要向指導教授台大醫工所 陳中明老師致上最高敬意與感謝。在研究所的求學與研究過程中，在陳老師的引領與指導下，我才有機會可以接觸到這些專業的領域並學習更多新的事物。陳老師治學嚴謹，成就卓越，並積極創新研究，認真嚴謹的研究精神與精準確實的研究態度，都讓我受益良多。

另外，我還要特別感謝台大醫院放射科 張允中醫師，張醫師提供了這次研究中最重要的數據與資料。並在過去的一年裡，在百忙之中還要抽空與我討論並一起參與實際的研究過程，甚至在週末也常犧牲他的假期與我一同解析與研究數據，由於他的協助與指導，讓我很快的增進有關醫學方面的知識。

在此一併感謝張醫師的助理雅琪小姐，在一些數據和報告上面也常幫我很多忙，讓我可以免於奔波與整理。還要感謝在展書樓研究室的眾學長姐和學弟妹，謝謝你們熱心的幫我解決一些研究上的小問題。並特別感謝在最後階段一直給我勉勵的慧真學姐和基展學長以及一同奮戰到最後的劍威。

在此特別感謝台大電機所的郭立威學長，承蒙他多年來的幫助讓我有勇氣持續面對各種艱困的挑戰，並得以完成我的夢想。

還要感謝秋芳，總是無怨無悔的陪伴與支持我的想法，是我在精神上的強力支柱，讓我可以勇往直前的追尋夢想。

最後更要謝謝我親愛的家人。父親與母親在研究所時期全力的支持我的想法並提供我無後顧之憂的資源，還有妹妹一直以來對家裡的幫忙，特別是到最後階段真的讓我很感動。

研究所生涯看似很長，其實一溜煙就過去了。那些喜悅和艱澀的回憶也將更豐富我的人生旅程，讓我更勇於面對未來的挑戰。

Albert 2008.08

中文摘要

動態對比增強磁共振影像(DCE-MRI)為一應用快速 MRI 掃瞄序列觀測身體內注射的對比劑進入血液中微灌流(perfusion)的情形。此應用對於觀察服用抗血管新增藥物病患的治療與評估有很顯著的成果。而對比劑進入人體血液循環系統到達腫瘤部位到代謝出來的行為模式往往可由不同的數學模型來描述。

目前有相當多的應用在於藉由量測這些數學模型的參數進而推得對比劑在循環系統或腫瘤組織附近的流動情形。由這些流動的難易程度亦可以非侵入方式估測腫瘤特性。

本研究的病人以肺癌病患為主，並施以 Avastin 抗癌藥物作為抗血管新增治療藥物。希望可以透過動態對比增強磁共振影像(DCE-MRI)的特性，早期預測並評估此抗癌藥物的化療效果。而本研究所採用的分析軟體 Mistar 可供我們選擇不同的數學模型來進一步評估治療的效果。

不過此軟體受限於本身功能的限制，對於肺部切面影像在掃瞄中的呼吸等自然位移與誤差未能進一步調整與修正。故本研究除了獲取動態對比增強磁共振影像(DCE-MRI)的數學模型參數外，更進一步提出影像前處理的方式來修正因為移動所造成的誤差影像。經過動態比對，修正後的影像有很明顯的改進。

除了影像位移的改進，另外我們也發現透過對於位移的校正，對這些動態對比增強磁共振影像(DCE-MRI)的數學模型參數之分佈曲線有很顯著且明顯的影響。因此位移效應之修正對於影像品質和參數之數值分佈有很重要的影響，我們希望這些影響對於此抗癌藥物的化療效果有指標性的評估作用。

關鍵詞：動態動比增強磁共振影像、藥物動力學數學模型、影像處理、位移校正。

Abstract

Dynamic-contrast-enhanced MRI (DCE-MRI) is the usage of fast pulse sequence MRI for monitoring the perfusion of contrast materials in the blood stream. This application is useful in evaluating patients taking angiogenesis inhibitors. The behavior of the contrast material in the blood stream can then be modeled using a variety of different mathematical models.

Currently, by measuring select data and employing the different mathematical models, it is possible to estimate the flow characteristics of the contrast materials in the blood stream as well as around the tumor. Subsequently, by using the different flow characteristics, it is possible to evaluate the tumor in a non-invasive way.

The patients in this study were lung cancer patients, and had been given Avastin. By employing DCE-MRI, it may be possible to predict and evaluate the effect of the chemotherapy early in the treatment course. This study employs Mistar, which is the software that provides the multitude of mathematical models for the evaluation treatment response.

Due to limitations of the software, however, inconsistencies resulting from image translation between tomography slices—due to spontaneous movements such as breathing—cannot be adjusted or corrected. Therefore, besides acquiring the DCE-MRI data for mathematical models, this study further employs image pre-processing for the correction of imaging errors due to subject movement. After dynamic comparison and correction, the image is vastly improved.

Besides improvements in image quality, translational correction also drastically improves the data used in the mathematical models. The usage of translational correction, therefore, greatly affects the final image quality, as well as the statistical

distribution of the data being measured. We hope these changes will have a landmark impact on the final evaluation of the effectiveness of the angiogenesis inhibitors as well.

Keywords：Dynamic Contrast Enhancement Magnetic Resonance Imaging, Tofts Model, Imaging processing, Motion Correction

Contents

論文口試委員審定書

誌謝 ……..i

中文摘要 ……ii

Abstract ……..iii

Contents …..…….…….....v

Lists of figures …….…….....vii

List of Tables …….…….....x

Chapter 1 Introduction

1.1 Dynamic Contrast Enhanced Magnetic Resonance Imaging ……...1

1.2 Tumor Angiogenesis ……3

1.3 Theory in DCE-MRI ……5

1.4 Pharmacokinetic Model ……..12

1.5 Tofts Model ……19

1.6 Application in DCE-MRI …….....24

Chapter 2 Theory in segmentation

2.1 Segmentation in normalized cuts method …….……..29

2.2 Gradient Vector Flow ……..…….....34

Chapter 3 Method

3.1 Clinical Experiment …….....38

3.2 Pre-processing in DICOM images ……..…….……..39

3.3 Mistar software processing ……..…….……..47

Chapter 4 Results

4.1 Results from Mistar software …….…….……50

4.2 Data Analysis …….……...57

Chapter 5 Discussion

5.1 Problems in Data Analysis ……...63

5.2 Inaccuracy Problems ……64

Chapter 6 Conclusion

6.1 Conclusion ..…….…….65

6.2 Future Work …….…….67

Reference ……68

Lists of Figures

Figure 1.1 The phenomenon about tumor angiogenesis ……...3

Figure 1.2 (a) Signal intensity curve before bolus injection. (b) Contrast agent is diffusion to the interstitial space. (c) After the first pass of the bolus, the SI increases further until the concentration of the contrast agent in the blood and the interstitial space of the tissue are equal. (d) After this equilibrium phase, the contrast medium is progressively washed out from the interstitial space as the arterial concentration decreases. ……..…… ..6

Figure 1.3 Angiogenesis starts with cancerous tumour cells releasing molecules, angiogenic promoter substances that send signals to surrounding normal host tissue. The small gray circles indicate contrast agent molecules. The contrast agent is administered as a single intravenous bolus injection at point 2. The contrast agent leaks into the extravascular-extracellular space (EES), also called the leakage space, through VVOs and widened interendothelial junctions (line 2 to line 3). At first the contrast agent accumulates in the extravascular tissue before it diffuses back into the vasculature from which it is excreted (line 3 to line 4). In an MR image the accumulation and wash-out of contrast agent is observed as changes in the MR signal intensity which is proportional to the concentration of contrast media. The time- intensity curve to the left in the fi gure shows the intensity of the MR signal from the zoomed region before (line 1 to line2) and after injection of contrast agent (line 2 to line 4). ……10

Figure 1.4 Three compartments in tracer kinetic model …….12

Figure 1.5 Illustration of General Kinetic Model ……...15

Figure 1.6 Illustration of Patlak Model ……..16

Figure 1.7 Illustration of Brix Model ……..……...18

Figure 1.8 Illustration of Tofts Model …..……..21

Figure 1.9 Contrast-enhanced magnetic resonance images (top row) and signal enhancement ratio (SER) parametric maps (bottom row), acquired before treatment (A), 2 weeks after the first cycle of doxorubicin-cyclophosphamide (B), and at the end of chemotherapy, before surgery (C), for a patient with locally advanced breast cancer.

Blue, green, and red color coding corresponds to low, moderate, and high values, respectively. ……..……..25

Figure 1.10 Columns show anatomic subtraction images, corresponding Transfer constant maps, and histograms from pixel data. Row shows data before treatment and after one and two cycles of mitoxantrone and methotrexate chemotherapy, respectively ……...…..28

Figure 2.1 A case where minimum cut gives a bad partition …….……....33

Figure 3.1 Image sequence in the clinical experiment …….……..38

Figure 3.2 Reference and Temporal images ……...…39

Figure 3.3 Registration problem in sequential images. …….…… 40

Figure 3.4 Adjust motion problem by moving temporal image to reference image …. 40

Figure 3.5 Select proper ROI in reference image. ……...…….. 41

Figure 3.6 Get proper ROI from the reference image to compare with the similar area in the temporal images ……..…….. 41

Figure 3.7 Contour which decided by user …… 42

Figure 3.8 Make outside gray level be zero ……... 42

Figure 3.9 Prepare proper ROI for normalize cut ...…….. …… 43

Figure 3.10 Results which determined by the normalize cut operation …….…..…….. 43

Figure 3.11 Four maps (test image, edge map, edge map gradient, normalized GVF field for determined gradient vector flow ……..…….……44

Figure 3.12 Running gradient vector flow program to determined the contour …….44

Figure 3.13 Final image which decided by normalize cut and gradient vector flow ….45

Figure 3.14 Correlation between reference and temporal image …….….. 45

Figure 3.15 Shift temporal images to the arbitrarily position which correlation value is maximum ……...… 46

Figure 3.16 Interface in operating Mistar software …….…….……. 47

Figure 3.17 Select processing area to in Mistar software. If we select large area, it will spend more time to finish the calculation. ……. 48

Figure 3.18 Processing the calculation (blue image is the area which selected to calculate) ……...……. 49

Figure 3.19 DCE-MRI parameter maps (upper right is v_e, upper left is k_{ep}, lower right is v_p, and lower left is k^{trans}) ……... 49

Figure 4.1 Select tumor contour by doctor to make sure the area is exactly in tumor position …… 50

Figure 4.2 Four parameters maps results which calculated by Mistar software, the yellow line in the pictures are the tumor position and shape decided by doctor …..…. 51

Lists of Tables

Table 1.1 Three Standard Kinetic Parameters ……..……..... 20

Table 1.2 Individual patient data showing tumour size, mean difference, coefficient of variation (CoV) and repeatability for K^{trans} and IAUC(60) for two scans …..…….. 26

Table 4.1 Four parameter values in each patient include the mean and standard deviation …… 53 ~ 56

Chapter 1 Introduction

1.1 Dynamic Contrast-Enhanced Magnetic Resonance Imaging

Dynamic contrast-enhanced magnetic resonance imaging (DCE-MRI) is a kind of MR images modality which over a period of time after the injection of contrast agent into vein. It's about computer-enhanced modality that relies on a special algorithm and mathematic model to estimate blood flow.

The DCE-MRI technique is based on the continuous acquisition of 2D or 3D MR images during the distribution of an paramagnetic contrast agent bolus. The contrast agent is a gadolinium-(Gd) based which is able to enter the extravascular extracellular space (EES) via the capillary bed. The pharmacokinetics of Gd distribution are modeled by a 2- or multi-compartment model and has been shown to be a useful predictor of the biological response of angiogenesis [1]. Many different methods for image acquisition and data analysis have been described for use in DCE-MRI. The analysis models are designed to derive the optimal relevant components from the dynamic MR signal changes and to relate these to the underlying physiological processes which are taking place in the tissue.

In particular, the dynamic contrast enhanced MRI combined with physiological model-based analysis has been widely used in the study of tumor angiogenesis and in

the development and trial of anti-angiogenesis drugs. The derivation of physiological data from dynamic contrast MRI relies on the application of appropriate pharmacokinetic models to describe the distribution of contrast media following its systemic administration [2].

1.2 Tumor Angiogenesis

Angiogenesis is a physiological process involving the growth of new blood vessels from pre-existing vessels. It's a normal process in growth and development, as well as in wound healing. However, this is also a fundamental step in the transition of tumors from a dormant state to a malignant state.

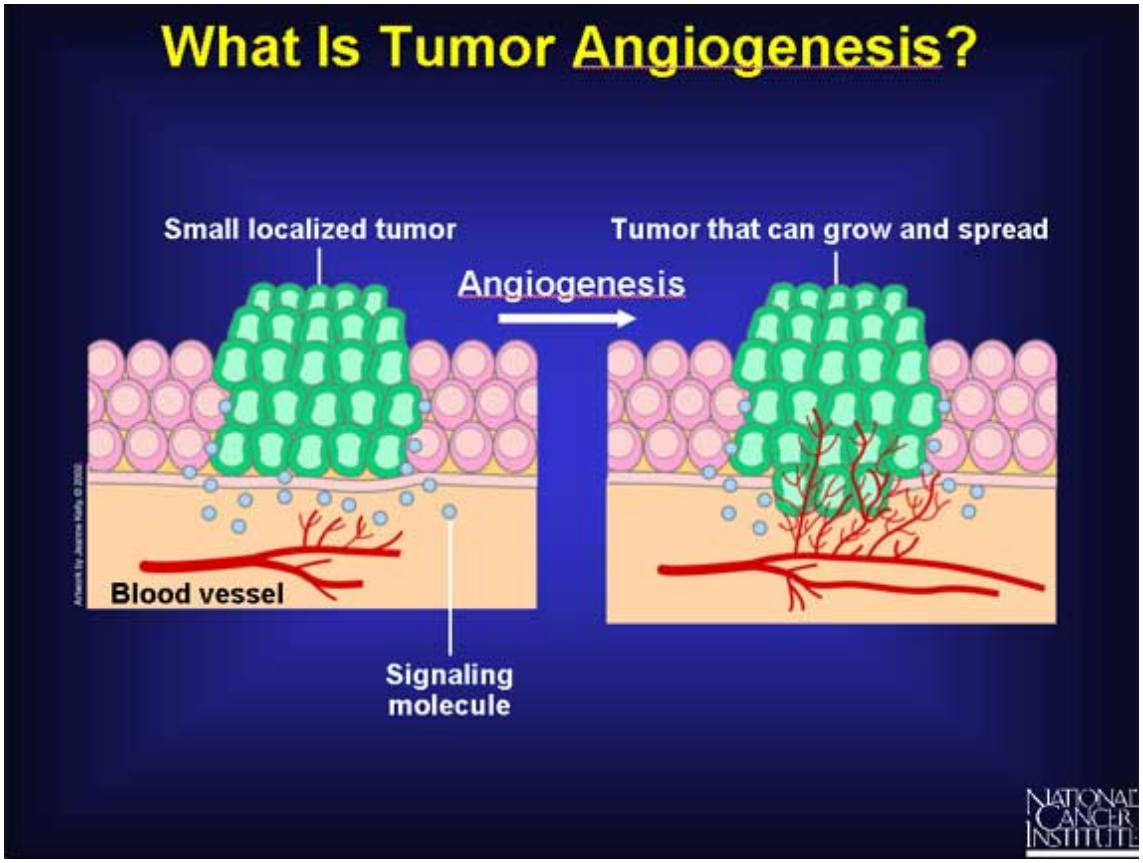

Fig 1.1 The phenomenon about tumor angiogenesis [3]

Tumor angiogenesis is the proliferation of a network of blood vessels that penetrates into cancerous growths (Fig 1.1), supplying nutrients and oxygen and removing waste products. Tumor angiogenesis actually starts with cancerous tumor cells releasing

molecules that send signals to surrounding normal host tissue. This signaling activates certain genes in the host tissue that, in turn, make proteins to encourage growth of new blood vessels [3]. The development of new blood vessels, is required for tumors to grow larger than 2-3 mm in size, and provided both nutrients and access to the systemic circulation with possible subsequent metastasis. This angiogenic process is mediated by several potent peptides, which include fibroblast growth factors and vascular endothelial growth factors [4].

Due to the characteristic in tumor angiogenesis, we can use the protocol of dynamic magnetic resonance imaging to measuring the tumor response indirectly.

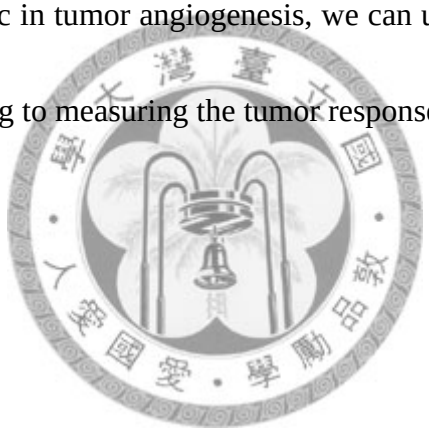

1.3 Theory in DCE-MRI

Dynamic contrast-enhanced MRI is a method of physiological imaging, based on fast or ultra-fast imaging, with the possibility of following the early enhancement kinetics of a water-soluble contrast agent after intravenous bolus injection. This technique provides clinically useful information, by depicting tissue perfusion, capillary permeability, and composition of the interstitial space. The most important advantages of this technique are its abilities to monitor response to preoperative chemotherapy, identify areas of viable tumor before biopsy, and provide physiological information for improved tissue characterization and detection recurrent tumor tissue after therapy [5].

The extracellular distribution of fluid MR contrast agents is among blood plasma and the interstitial spaces. When a contrast agent is administered intravenously by a rapid bolus injection, it is first diluted in the blood of the peripheral vein and the right heart, before it passes through the lungs and the left heart into the peripheral circulation (Fig. 1.2a).

During first pass of the contrast agent through the capillaries, a fast diffusion occurs into the tissue, due to the high concentration gradient between the intravascular and the interstitial space: in normal tissues, approximately 50% of the circulating contrast agent diffuses from the blood into the extravascular compartment during the first pass.

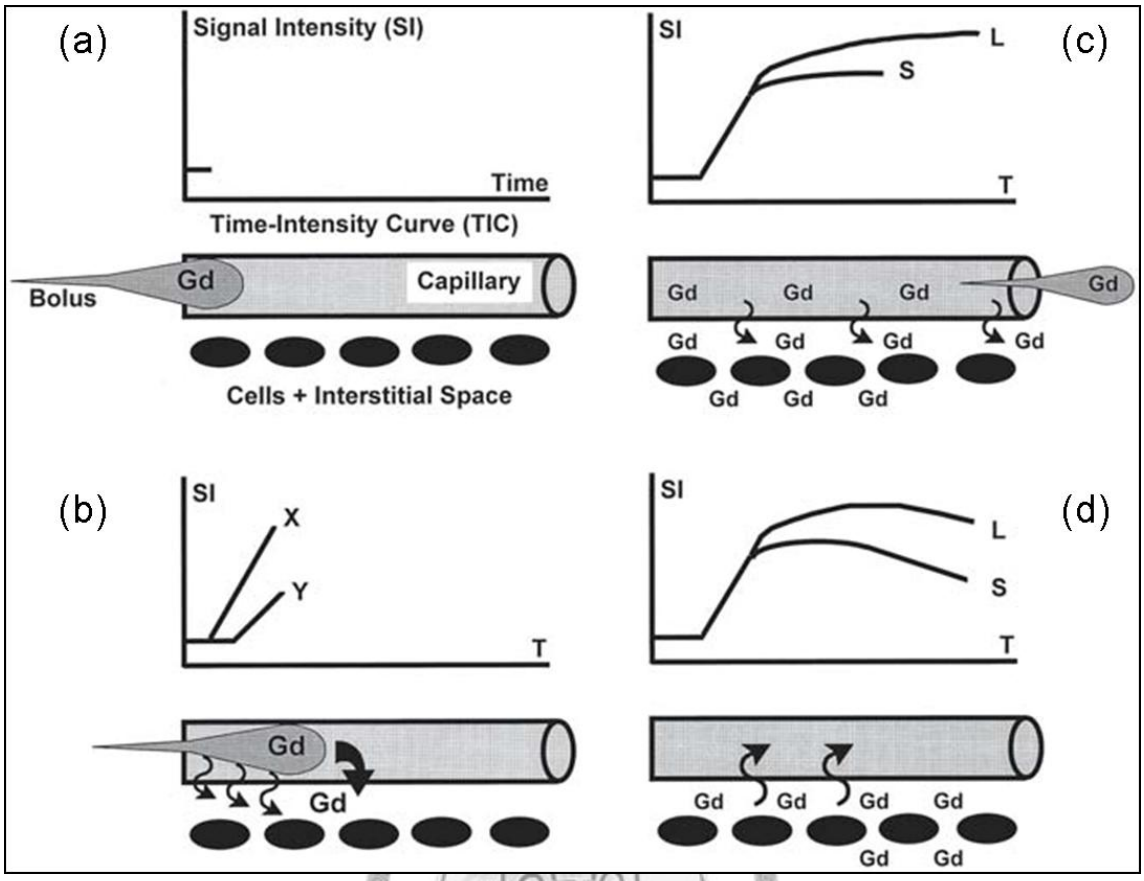

Fig 1.2 (a) Signal intensity curve before bolus injection. (b) Contrast agent is diffusion to the interstitial space. (c) After the first pass of the bolus, the SI increases further until the concentration of the contrast agent in the blood and the interstitial space of the tissue are equal. (d) After this equilibrium phase, the contrast medium is progressively washed out from the interstitial space as the arterial concentration decreases. [5]

This first-pass diffusion is essentially different from that during the second pass and later. At this initial moment, there is no contrast agent in the interstitial space, and the agent has its highest possible plasma concentration, because it is diluted in only a very small part of the total plasma volume, namely that volume that enters into the right side of the heart at the same time as the bolus (Fig. 1.2b).After the first pass, the diffusion rate immediately drops, because the concentration of the re-circulating contrast medium has decreased owing to further dilution in the blood and partial accumulation in the

interstitial space throughout the body. The length of the time interval between the end of the first pass and the equilibrium state, with equal concentrations of contrast medium in plasma and interstitial space, depends on the size of the interstitial space (Fig. 1.2c). After this equilibrium phase, the contrast medium is progressively washed out from the interstitial space as the arterial concentration decreases (Fig. 1.2d).

Only in highly vascular lesions with a small interstitial space does early washout occur within the first minutes after bolus injection. The aim of dynamic contrast enhance MRI is detect and depict differences in early intravascular and interstitial distribution as this process is influenced by pathological changes in tissues [5].

Numerous studies using dynamic contrast enhanced MRI have demonstrated that malignant tumors generally show faster and higher levels of enhancement than is seen in normal tissue. This enhancement characteristic reflects the features of the tumor microvasculature which in general will tend to demonstrate increased proportional vascular and higher endothelial permeability to the contrast molecule than do normal or less aggressive malignant tissues.

Cancer can develop in any tissue of the body that contains cells capable of division. The earliest detectable malignant lesions, referred to as cancer are often a few millimeter or less in diameter and at an early stage. In vascular tumors cellular nutrition depends on diffusion of nutrients and waste materials and places a severe limitation on

the size that such a tumor can achieve.

Conversion of a dormant tumor to a more rapidly growing invasive neoplasm, may take several years and is associated with visualization of the tumor. The development of neovascularization within a tumor results from a process known as angiogenesis.

These angiogenically competent cells have the ability to induce neovascularization through the release of angiogenic factors. There are positive and negative regulators of angiogenesis. Release of a promoter substance stimulates the endothelial cells of the existing vasculature close to the neoplasia to initiate the formation of solid endothelial sprouts that grow toward the solid tumor [2].

The following figure (Fig 1.3) illustrate the concept from tumor cell angiogenesis to the MRI signal intensity curve during the process of inject contrast agent. (a) Growth of a malignant tumor depends on its ability to stimulate neighboring vasculature to initiate formation of new blood vessels that can grow into the tumor and supply it with oxygen and nutrients. Angiogenesis starts with cancerous tumor cells releasing molecules, angiogenic promoter substances that send signals to surrounding normal host tissue. These signals activate certain genes in the host tissue that, in turn, make proteins to encourage growth of new vessels. A new blood capillary can form by sprouting of endothelial cells from the wall of an existing small vessel. The cells at first form a solid sprout, which then hollows out to form a tube. This process continues until the sprout

encounters another vessel, with which it connects, allowing blood to circulate.

(b) The resolution of an MR image is determined by the field of view (FOV) and the matrix size. The pixel size and the thickness of the image slice give the volume of the voxel shown in the figure. One voxel contains many different cells even when using the smallest FOV and the largest matrix size possible. This means that the MR signal obtained from one voxel is the average of the proportion of tissue covered by the voxel.

(c) The zoomed region shows a cross section through a blood vessel and the surrounding extravascular tissue consisting of tumor cells, extracellular components and normal cells. The vessel wall is mainly made up of endothelial cells. The small grey circles indicate contrast agent molecules. The contrast agent is administered as a single intravenous bolus injection at point 2. The contrast agent leaks into the extravascular-extracellular space (EES), also called the leakage space (line 2 to line 3). How fast the contrast agent extravasates is determined by the permeability of the microvessels, their surface area, and the blood flow.

At first the contrast agent accumulates in the extravascular tissue before it diffuses back into the vasculature from which it is excreted. It usually by the kidneys, although some contrast media have significant hepatic excretion (line 3 to line 4). In an MR image the accumulation and wash-out of contrast agent is observed as changes in the MR signal intensity which is proportional to the concentration of contrast media.

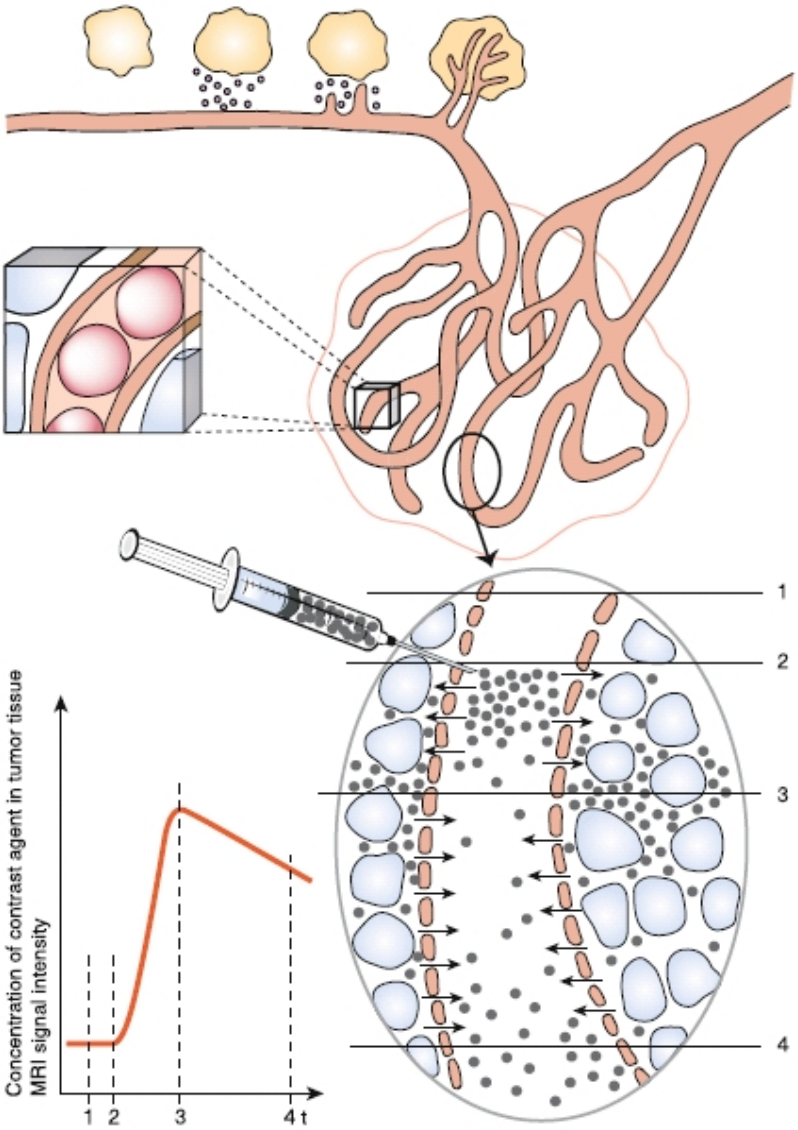

Fig 1.3 Angiogenesis starts with cancerous tumour cells releasing molecules, angiogenic promoter substances that send signals to surrounding normal host tissue. The small gray circles indicate contrast agent molecules. The contrast agent is administered as a single intravenous bolus injection at point 2. The contrast agent leaks into the extravascular-extracellular space (EES), also called the leakage space, through VVOs and widened interendothelial junctions (line 2 to line 3). At first the contrast agent accumulates in the extravascular tissue before it diffuses back into the vasculature from which it is excreted (line 3 to line 4). In an MR image the accumulation and wash-out of contrast agent is observed as changes in the MR signal intensity which is proportional to the concentration of contrast media. The time- intensity curve to the left in the fi gure shows the intensity of the MR signal from the zoomed region before (line 1 to line2) and after injection of contrast agent (line 2 to line 4). [2]

The time-intensity curve to the left in the figure shows the intensity of the MR signal from the zoomed region before (line 1 to 2) and after injection of contrast agent (line 2 to line 4)

The mechanisms underlying the signal enhancement patterns seen on dynamic MRI include variations in regional blood flow, proportional blood vessel density, vascularization of existing blood vessels and variations in the surface area permeability of the endothelial membranes as well as the concentration difference which exists between plasma and the EES [2].

In many tumor types including breast, lung, prostate, and head and neck cancer, measurements of microvascular density made on histopathological samples correlate closely with clinical stage and act as an independent prognostic factor of considerable sensitivity. The rationale for this relationship appears to be that rapid tumor growth can be supported only in the presence of highly active angiogenesis and more aggressive tumor are therefore associated with increased evidence of angiogenesis-related microvasculature abnormalities. On the basis of this histopathological evidence it has been suggested that dynamic contrast enhanced MRI may also be able to provide independent indices of angiogenic activity and therefore act as a prognostic indicator in a broad range of tumour types [2].

1.4 Pharmacokinetic Model

When we want to attempt to quantify the observed contrast agent kinetics in terms of physiologically meaningful parameters we first need to define the elements of the tumor or tissue structure and the functional processes that affect the distribution of the tracer (the contrast agent). It is customary to represent tissue as comprising three or four compartments, each of which is a bulk tissue characteristic (we are unable to observe these compartments at their natural microscopic scale, but we can observe their aggregate effects at the image voxel scale or in a region of interest).

These compartments are the vascular plasma space, the extracellular extravascular space (EES), and the intracellular space (Fig. 1.4).

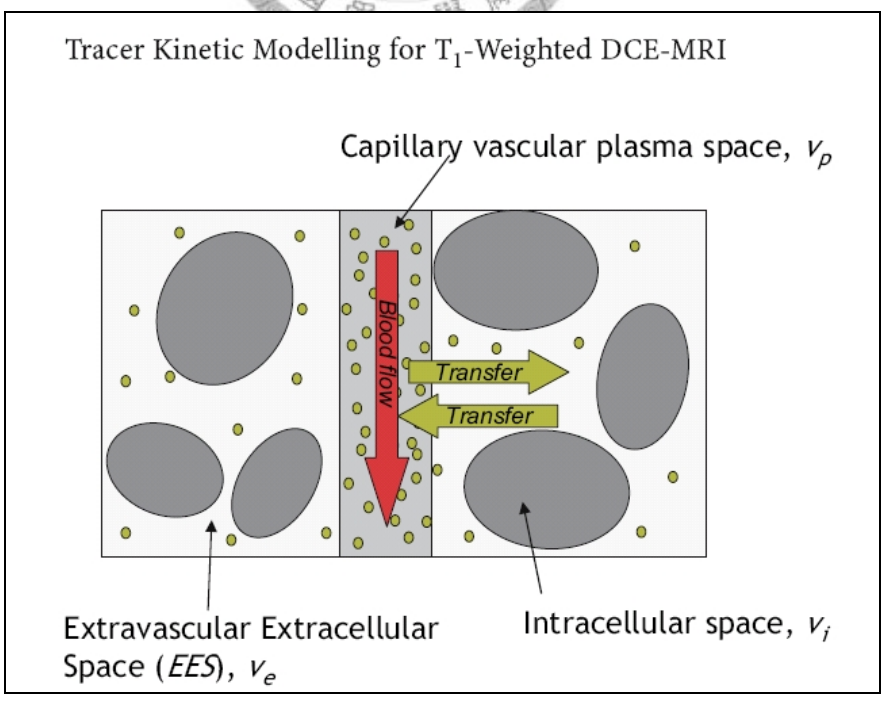

Fig 1.4 Three compartments in tracer kinetic model. [2]

All clinically utilized MRI contrast agents, and most experimental agents, are not pass into the intracellular space of the tissue due to their size, inertness, and non-lipophilicity, making the intracellular space un-probable using DCE-MRI; for this reason, the intracellular and other volumes are usually lumped together as a loosely defined intracellular space. According to fig 1.4 we can get the relationship between these compartments:

$$V_e + V_p + V_i = 1 \tag{1.1}$$

$$V_p = (1 - Hct)V_b \tag{1.2}$$

where V_e is the fractional EES, V_p is the fraction occupied by blood plasma, V_i is the fraction occupied by the intracellular space, V_b is the fraction occupied by whole blood, and Hct is the haematocrit (typically about 0.4).

The functional parameters, or delivery mechanisms, that influence contrast agent distribution in the intravascular space and the EES are usually assumed to be restricted to blood flow F and the endothelial permeability surface area product PS, which describe how leaky a capillary wall is.

There are two physiological processes that accompany the faster growth rate of many tumors: an increased number of vessels and along with an increased permeability. Therefore, one could expect an increased overall signal enhancement in the vicinity of tumors due to increasing vascular volume, vessel permeability, and increased flow.

In the simplest model of tissue signal enhancement characteristics one could describe 3 parameters: maximum signal enhancement, the rate at which this initial enhancement occurs "wash-in", and the rate at which this increased signal decays "wash-out". However, it is important to consider this contrast dynamic with respect to the concentration of contrast agent in the vascular system as it perfusion the tissues. In simple graphical wash-in wash-out, it is assumed that the contrast agent immediately reaches equilibrium in the vascular system [6].

The data obtained with DCE-MRI is reported semi quantitatively using parameters derived from pharmacokinetic models. Quantitative techniques that are often combined with rapid temporal sampling have been used together with simple pharmacokinetic models of tissues, obtaining parameters such as the transfer constant (K^{trans}), the rate constant (k_{ep}), and v_e.

Most MRI kinetic models were developed from Nuclear Medicine quantitative studies but the limitations of MRI dictated specific modifications. A number of these MRI models are in current use, the primarily differentiated based on the way that they model the "arterial input function" (AIF).

1.4.1 General Kinetic Model

The General Kinetic Model (GKM) is one approach to understanding the complex

kinetics of contrast enhancement. The physiological processes of GKM are described in Figure 1.5, where the GKM simplifies the anatomy of the tumor into two functional components, the vascular space and the EES and one non-functional component, the intracellular space.

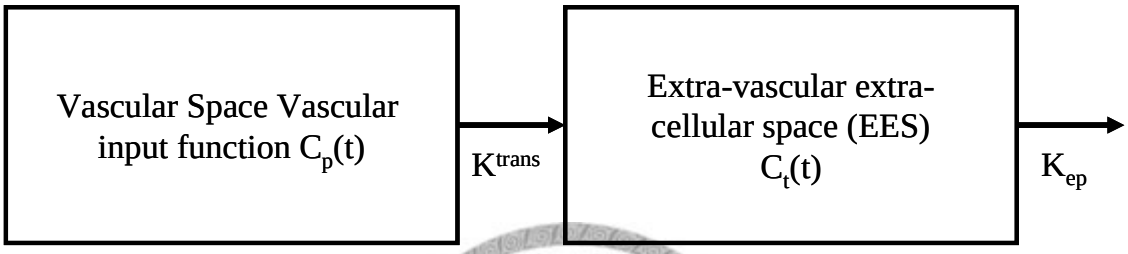

Fig 1.5 Illustration of General Kinetic Model [6]

A contrast agent, specifically a highly diffusible low molecular weight agent which remains extracellular, when introduced into the vascular space will leak into the EES at a characteristic rate and then will leak back into the vessel at another rate. Thus the net change in concentration in the tumor can be described as:

$$\frac{dC_t}{dt} = K^{trans} C_p - k_{ep} C_t \qquad (1.3)$$

where K^{trans} is a factor related to "wash in" and k_{ep} is a factor related to "wash-out" and the relationship between these parameters was the volume of extravascular-extracellular space v_e. Furthermore, we can numerically evaluate these parameters for a variable concentration input function. This expression is mathematically described as a convolution integral.

$$C_t(t) = K^{trans}[C_p(t) \otimes e^{k_{ep}t}] \quad (1.4)$$

This equation gives the relationship of the rate of change in tumor concentration at any given time after contrast administration to the plasma and tumor concentration at that time. A numerical solution for the GKM (K^{trans} and k_{ep}) can be obtained by a nonlinear fitting algorithm for this expression. Subsequent models are based on this general model, but use various assumptions to work around the convolution integral.

1.4.2 Patlak Model

Another approach to determining vessel permeability from time concentration curves was proposed by Patlak [7]. It uses a graphical method to estimate permeability surfaces and fractional vascular space based on the slope and intercept of a derived line. Figure 1.6 describes the physiological processes of the Patlak model in a block format.

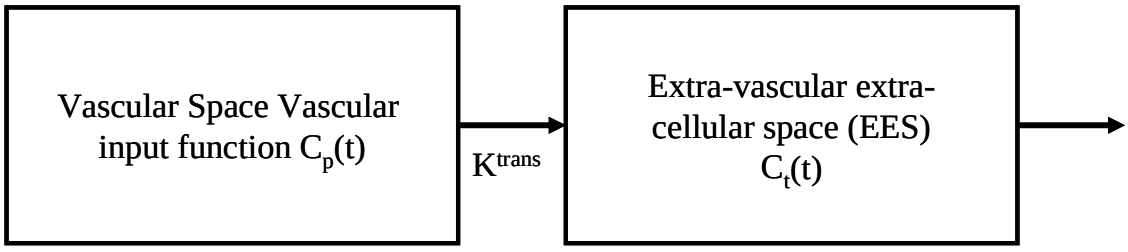

Fig 1.6 Illustration of Patlak Model [7]

In this method, flow from the tissue space to the vascular space is assumed negligible and flow is assumed to be unidirectional. In this model, the contrast agent in

the tumor can be expressed as:

$$C_t(t) = K^{trans}\int_0^t C_p(\tau)d\tau + v_p C_p(t) \qquad (1.5)$$

where v_p is the fractional plasma volume. The term is similar in concept to the term v_e. Dividing both sides of the equation by $C_p(t)$ yields:

$$\frac{C_t}{C_p} = K^{trans}\frac{\int_0^t C_p(\tau)d\tau}{C_p} + v_p \qquad (1.6)$$

The Patlak approach utilizes a simpler approach than the standard pharmacokinetic model. A major advantage of the Patlak model is based in its incorporation of AIF. However one limiting assumption of this model is that the contrast agent flows only into the tissue of interest. If the slope of the "Patlak" graph is not linear, then the assumption of no back flow is violated and the parameters generated would no longer be valid.

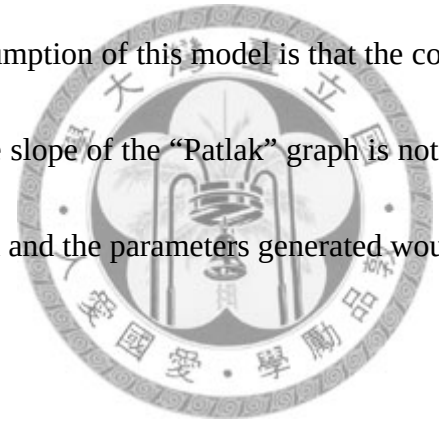

1.4.3 Brix Model

Brix model is also a two compartment model in which the arterial input curve is assumed to be the result of a prolonged constant infusion that takes the shape of square wave (i.e. the contrast agent instantly reaches a plateau, remains constant for awhile and then instantly is over) which mixes in the vascular space and is slowly eliminated by renal excretion [8]. The input function is of magnitude K_{in}, the elimination constant is k_{el}, and the rate constants describing the transfer of contrast agent from plasma to the tumor space and back are k_{12} and k_{21}.

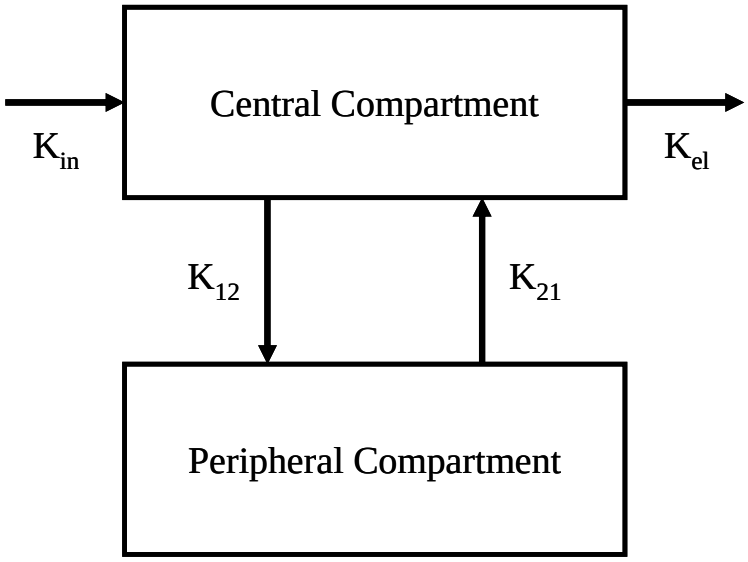

Fig 1.7 Illustration of Brix Model. [8]

The mathematical expression of the temporal response of S_{CM} (t) / S_0 is obtained:

$$\frac{S_{CM}(t)}{S_0} = 1 + A\left\{v\left[e^{(k_{el}t')} - 1\right]e^{(k_{el}t)} - u\left[e^{(k_{21}t')} - 1\right]e^{(k_{21}t)}\right\} \qquad (1.7)$$

Where S_{CM} (t) is the time–independent Gd-DTPA enhanced MRI signals, A is a fitting parameter depending on the properties of the tissue of the sequence used, and of the infusion rate (K_{in}). Brix put forth a mathematical description that incorporated a term that allowed the adjustment of an AIF parameter.

1.5 Tofts Model

Tofts model takes a different approach to the arterial input function (AIF), but retains the fundamental assumptions of the GKM (General Kinetic Model) [9],[10]. In the Tofts model, the input function is assumed to be the result of a pulse bolus injected into a two compartment system.

The arterial input is modified by diffusion transfer of contrast material between the vascular space and body extravascular space; this system of compartments modifies the pulse bolus into a biexponential arterial input function [11].

This model consists of two parts: a compartmental model to establish the time course of the contrast agent (Gd-DTPA) tracer concentration in the tissue; and relate to observed MRI signal enhancement.

A compartmental model is used to model the concentration of tracer with time. It consists of a plasma volume, connected to a large extracellular space which is distributed throughout most of the body (e.g., muscle). The kidneys drain tracer from the plasma, and hence from the extracellular space. We have modified this model by adding a fourth compartment, the lesion, which is connected to the plasma through a leaky membrane (Fig 1.8).

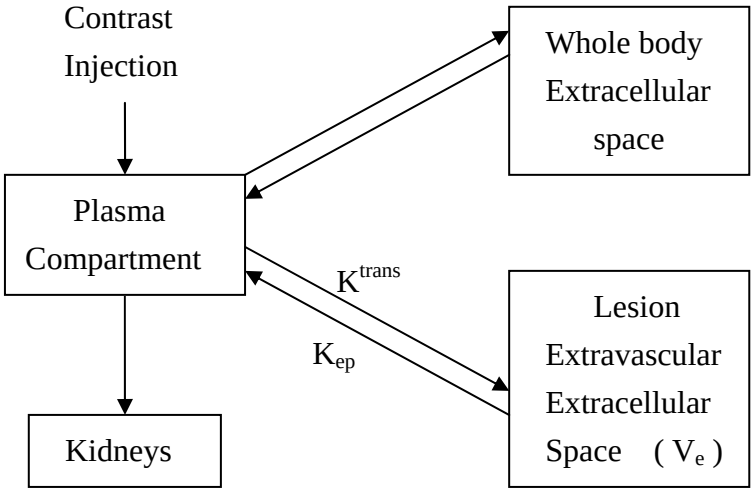

Fig 1.8 Illustration of Tofts Model.

Most methods of analyzing dynamic contrast-enhanced T1-weighted data have used a compartmental analysis to obtain some combination of the three principle parameters: the transfer constant (K_{trans}), the extravascular extracellular space (EES) fractional volume (v_e), and the rate constant (k_{ep}).

Three Standard Kinetic Parameters		
Symbol	Preferred short name	Full name
K^{trans}	Transfer Constant	Volume transfer constant between blood plasma and EES
k_{ep}	Rate Constant	Rate constant between EES and blood plasma
v_e	EES	Volume of extravascular extracellular space per unit volume of tissue

Table 1.1 Three Standard Kinetic Parameters.

Most methods of analyzing dynamic contrast-enhanced T1-weighted data have used a compartmental analysis to obtain some combination of the three principle parameters: the transfer constant (K^{trans}), the extravascular extracellular space (EES) fractional volume(v_e), and the rate constant (k_{ep}). The transferconstant and the EES relate to the fundamental physiology, whereas the rate constant is the ratio of the transfer constant to the EES [10]:

$$K_{ep} = \frac{K^{trans}}{v_e} \tag{1.8}$$

The rate constant can be derived from the shape of the tracer concentration vs time data, whereas the transfer constant and EES require access to absolute values of tracer concentration. The transfer constant K_{trans} has several physiologic interpretations, depending on the balance between capillary permeability and blood flow in the tissue of interest.

In high permeability, transfer constant is equal to the blood plasma flow per unit volume of tissue:

$$K^{trans} = F\rho(1 - Hct) \qquad \text{(PS >> F)} \tag{1.9}$$

Where ***F*** are Perfusion (or flow) of whole blood per unit mass of tissue, ρ means the density of tissue, ***Hct*** represent for Hematocrit, ***P*** means total permeability of capillary wall, S means surface area per unit mass of tissue.

In the other limiting case of low permeability, where tracer flux is permeability

limited, the transfer constant is equal to the permeability surface area product between blood plasma and the EES, per unit volume of tissue [12]:

$$K^{trans} = PS\rho \qquad (PS << F) \qquad (1.10)$$

Tracer flows passively from the blood plasma in a permeable capillary into the EES, through microscopic pores or defects in the capillary walls. It also called the interstitial space.

The rate constant k_{ep} is formally the flux rate constant between the EES and blood plasma. It's always greater than the transfer constant K^{trans}. For a range of typical EES fractional volumes seen in tumors and multiple sclerosis (v_e = 20% ~ 50%), k_{ep} is two to five times higher than K^{trans} [10].

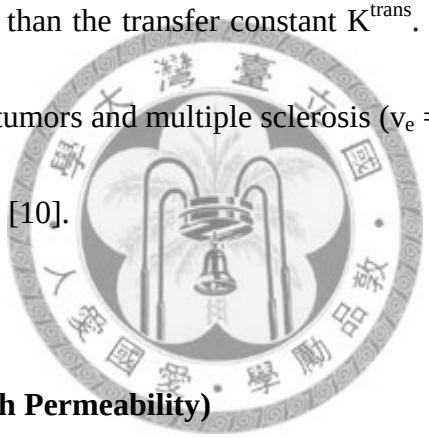

Flow-Limited Model (High Permeability)

Its first assumption is that arterial and venous blood have well-defined concentrations, supplying and draining the tissue under study. Second, because permeability is high, venous blood leaves the tissue with a tracer concentration that is at all times in equilibrium with the tissue. Thus, soon after injection of the tracer, the arterial concentration is high, the venous concentration is low, and most of the tracer is being removed from the blood as it passes through the tissue.

For an extracellular tracer, the model can be extended by setting the venous

concentration equal to that of the EES. The effect of intravascular tracer on the MR signal can be ignored (ie, the vascular signal is small compared with the tissue signal). In this case the following differential equation relating tissue concentration C_t to arterial plasma concentration C_p can be obtained:

$$\frac{dC_t}{dt} = F\rho(1-Hct)(C_P - \frac{C_t}{v_e}) \quad (1.11)$$

PS-Limited Model (Low Permeability)

If flow is high, the blood plasma can be considered as a single pool, with equal arterial and venous concentrations. The transport of tracer out of the vasculature is slow enough not to deplete the intravascular concentration.

The rate of uptake is then determined by the permeability surface area product of the capillary wall and the difference between the blood plasma concentration and the EES concentration. If the contribution of tracer in the intravascular space is ignored, the transport equation is

$$\frac{dC_t}{dt} = PS\rho(C_P - \frac{C_t}{v_e}) \quad (1.12)$$

1.6 Application in DCE-MRI

Dynamic contrast-enhanced magnetic resonance imaging (DCE-MRI) is being used in oncology as a noninvasive method for measuring properties of the tumor microvasculature.

For DCE-MRI to be used as a biomarker, the method for quantifying the assay has to be defined. There are several goals to be weighed in optimizing the biomarker definition. The biomarker needs to (1) maximize the sensitivity to biologic changes caused by treatment; (2) capture tumor heterogeneity, which is an important as a biomarker [13].

Fig 1.9 is an illustration of parametric analysis of DCE-MRI images using an empirical parameter, the SER, for a patient with locally-advanced breast cancer treated with doxorubicin-cyclophosphamide (AC) chemotherapy. MRI was performed before chemotherapy, 2 weeks after the first cycle of chemotherapy, and at the end of AC treatment, before surgery, using a three–time point DCE-MRI method.

Pharmacokinetic properties of the tumor were quantified by computing SER at each pixel, defined as SER＝(S1-S0)/(S2-S0), where S0, S1 and S2 are the pre-contrast (baseline), early post-contrast and late post-contrast signal intensities.

DCE-MRI is a promising biomarker candidate for assessing antiangiogenic treatment. Correlative studies performed in combination with therapeutic trials have

demonstrated proof of concept for DCEMRI as a biomarker; however they have not been powered to adequately evaluate biomarker performance [13].

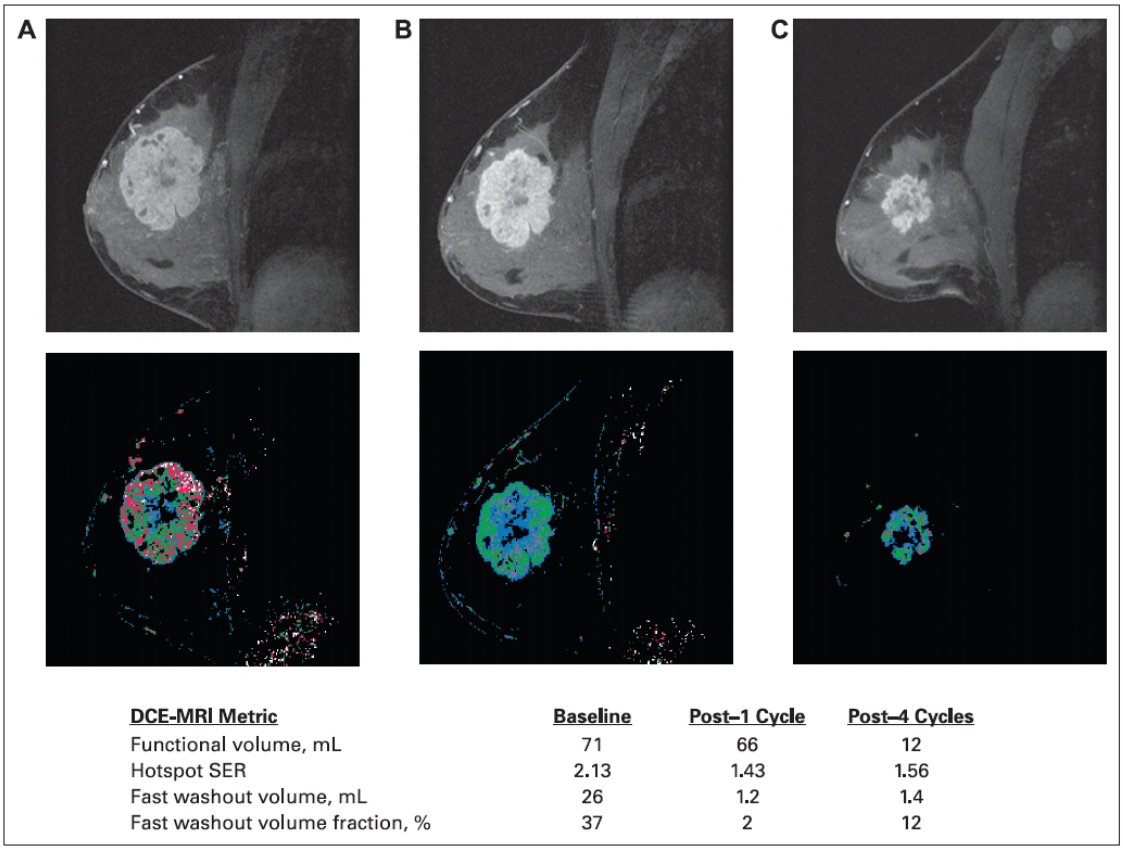

DCE-MRI Metric	Baseline	Post–1 Cycle	Post–4 Cycles
Functional volume, mL	71	66	12
Hotspot SER	2.13	1.43	1.56
Fast washout volume, mL	26	1.2	1.4
Fast washout volume fraction, %	37	2	12

Fig 1.9 Contrast-enhanced magnetic resonance images (top row) and signal enhancement ratio (SER) parametric maps (bottom row), acquired before treatment (A), 2 weeks after the first cycle of doxorubicin-cyclophosphamide (B), and at the end of chemotherapy, before surgery (C), for a patient with locally advanced breast cancer. Blue, green, and red color coding corresponds to low, moderate, and high values, respectively. [13]

Another paper demonstrates a single slice imaging technique. The image acquisition is performed in less than 500 ms making it relatively insensitive to respiratory motion. Data from phantom studies and a reproducibility study in solid human tumor. The reproducibility study showed a coefficient of variation (CoV) of 19.1% for K_{trans} and 15.8% for the initial area under the contrast enhancement curve (IAUC). This was

improved to 16 and 13.9% if tumor of diameter less than 3 cm were excluded. The individual repeatability was 30.6% for K^{trans} and 26.5% for IAUC for tumor which are greater than 3 cm diameter [14].

The individual patient data for two commonly used parameters, K^{trans} and IAUC (60), calculated from R1 values, are given in Table 1.2. Although no correlation was seen between T2 signal intensity and enhancement parameters, the second case in Table 1.2 had very high T2 compared with the other cases, consistent with a cystic nature of the metastasis. Guidelines from a recent US national cancer institute workshop on DCE–MRI state that tumors in a fixed superficial location should be at least 2 cm in diameter and other tumors should be at 3 cm in diameter. This study shows a tendency for greater variability with reducing size, and excluding lesions less that 3 cm in diameter reduced CoV.

			K^{trans} (min^{-1})			IAUC(60)		
Site	Primary	Size (cm)	Scan 1	Scan 2	% change	Scan 1	Scan 2	% change
Liver	Colorectal	7	0.116	0.111	−4.3	10.1	9.7	−3.7
Liver	Colorectal	2.8	0.018	0.014	−22.2	1.2	1.1	−15.2
Liver	Colorectal	4.7	0.116	0.100	−14.0	9.3	8.2	−11.6
Liver	Colorectal	6	0.186	0.192	3.2	16.6	15.1	−9.1
Liver	Colorectal	10.4	0.037	0.044	18.9	3.6	4.2	15.6
Liver	Colorectal	17	0.085	0.081	−4.7	6.7	6.7	−0.5
Liver	Lung	4.6	0.039	0.051	30.8	3.5	4.3	24.1
Lung	Lung	2.5	0.231	0.298	29.0	17.4	21.0	20.8
Lung	Lung	7	0.152	0.171	12.5	12.6	14.5	15.0
Lymph node	Melanoma	2.4	0.49	0.40	−18.5	35.0	28.7	−18.0
			K^{trans}			IAUC(60)		
All cases	Mean change (%)		3.1			1.7		
	CoV (%)		19.1			15.8		
	Repeatability (%)		36.1			29.5		
Size > 3 cm	Mean change (%)		6.1			4.3		
	CoV (%)		15.5			13.9		
	Repeatability (%)		30.6			26.5		

Table 1.2 Individual patient data showing tumour size, mean difference, coefficient of variation (CoV) and repeatability for K^{trans} and IAUC(60) for two scans.[14]

The colorectal liver metastases group also had lower CoV and repeatability values (K^{trans} 14.2 % and 26.5% and IAUC(60) 11 % and 21.3%, respectively), although this may be related to the fact that this group had relatively larger tumor.

Another approach explore the randomized trials confirm these benefits and show equivalent survival for adjuvant and neo-adjuvant chemotherapy in patients with primary operable breast cancer [16-17]. A further benefit of neo-adjuvant chemotherapy is the opportunity to assess the chemo-responsiveness of the tumor. The overall response rates reported vary between 60% and 100%, with complete clinical responses ranging from 10% to almost 50%, avoiding mastectomy in most cases. Clinical responders have a better prognosis than do non-responders [18].

The prognostic importance of histo-pathologic response among patients undergoing neo-adjuvant chemotherapy for breast cancer is also recognized [19]. Patients who have complete pathologic response or pathologic minimal residual disease have a longer disease-free and overall survival compared with patients who have gross residual disease. The ability to identify non-responders early after the start of chemotherapy would be of major benefit because it would enable treatment to be adjusted or enable alternative and possibly more efficacious treatments, such as other types of chemotherapy or early surgery, to be offered as soon as possible [20].

Fig 1.10 shows the change in transfer constant in perimenopausal woman with a

grade 3 infiltrating ductal carcinoma of the left breast not responding to mitoxantrone and methotrexate chemotherapy.

After one cycle of treatment (middle row), an increase in the transfer constant median and range is seen (57% and 34%, respectively), compared with a 10% decrease in tumor size. After two treatments (bottom row), a further increase in the transfer constant median and range is seen (186% and 181%, respectively) on the transfer constant histogram, compared with a 11% increase in tumor size [21].

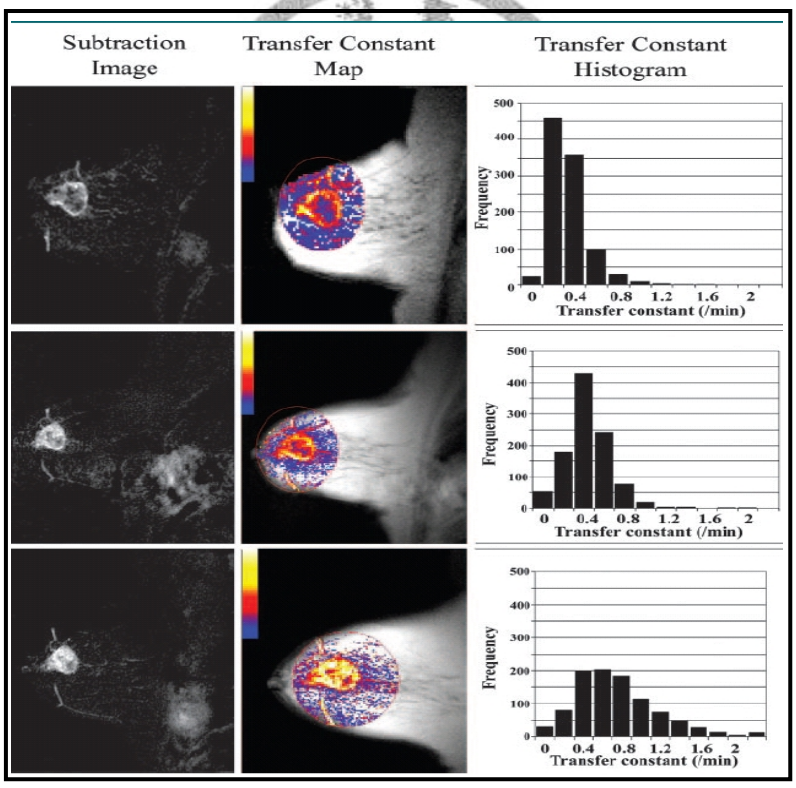

Fig 1.10 Columns show anatomic subtraction images, corresponding Transfer constant maps, and histograms from pixel data. Row shows data before treatment and after one and two cycles of mitoxantrone and methotrexate chemotherapy, respectively. [21]

Chapter 2 Theory in Segmentation

2.1 Segmentation in normalized cuts method

Segmentation refers to the process of partitioning a digital image into multiple regions. The goal of segmentation is to simplify or change the representation of an image into something that is more meaningful and easier to analyze [22]. Image segmentation is typically used to locate objects and boundaries (lines, curves, etc.) in images. The result of image segmentation is a set of regions that collectively cover the entire image, or a set of contours extracted from the image. Each of the pixel in a region are similar with respect to some characteristic or computed property, such as color, intensity, or texture.

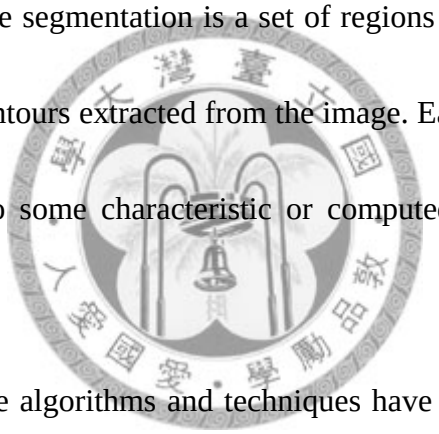

Several general-purpose algorithms and techniques have been developed for image segmentation. Since there is no general solution to the image segmentation problem, these techniques often have to be combined with domain knowledge in order to effectively solve an image segmentation problem.

The “normalized cuts” method was first proposed by Shi and Malik in 1997[23] . In this method, the image being segmented is modeled as a weighted undirected graph. Each pixel is a node in the graph, and an edge is formed between every pair of pixels. The weight of an edge is a measure of the similarity between the pixels. The image is

partitioned into disjoint sets by removing the edges connecting the segments. The optimal partitioning of the graph is the one that minimizes the weights of the edges that were removed (the "cut"). Shi's algorithm seeks to minimize the "normalized cut", which is the ratio of the "cut" to all of the edges in the set.

The normalized cut criterion measures both the total dissimilarity between the different groups as well as the total similarity within the groups. The grouping algorithm consists of the following steps:1. Given an image or image sequence, set up a weighted graph G = (V,E) and set the weight on the edge connecting two nodes to be a measure of the similarity between the two nodes. 2. Solve …(D-W)x = λ Dx for eigenvectors with the smallest eigenvalues. 3. Use the eigenvector with the second smallest eigenvalue to bipartition the graph. 4. Decide if the current partition should be subdivided and recursively repartition the segmented parts if necessary.

A graph G = (V,E) can be partitioned into two disjoint sets, A and B, by simply removing edges connecting the two parts. The degree of dissimilarity between these two pieces can be computed as total weight of the edges that have been removed. In graph theoretic language, it is called the cut :

$$cut(A, B) = \sum w(u, v) \qquad (2.1)$$

The optimal of a graph is the one that minimizes this cut value. Although there are an exponential number of such partitions, finding the minimum cut of a graph is a

well-studied problem and there exist efficient algorithms for solving it. Wu and Leahy [24] proposed a clustering method based on this minimum cut criterion. In particular, they seek to partition a graph into k-subgraphs such that the maximum

cut across the subgroups is minimized.

This problem can be efficiently solved by recursively finding the minimum cuts that bisect the existing segments. As shown in Wu and Leahy's work, this globally optimal criterion can be used to produce good segmentation on some of the images.

However, as Wu and Leahy also noticed in their work, the minimum cut criteria favors cutting small sets of isolated nodes in the graph. This is not surprising since the cut defined in (1) increases with the number of edges going across the two partitioned parts. Fig. 2.1 illustrates one such case.

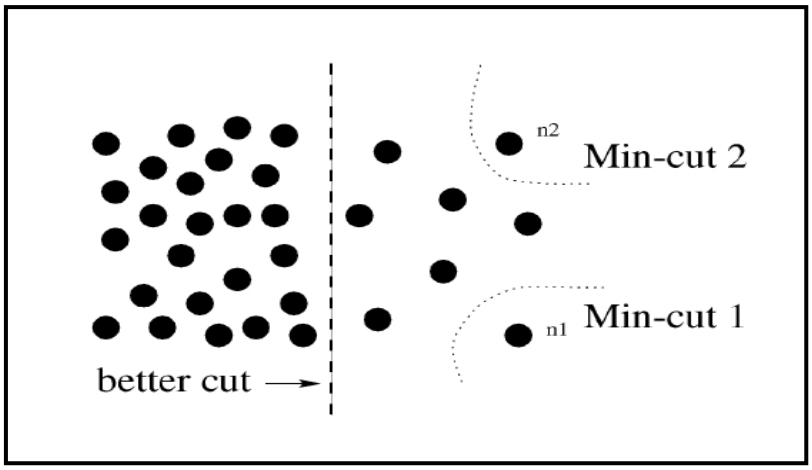

Fig 2.1 A case where minimum cut gives a bad partition. [23]

Assuming the edge weights are inversely proportional to the distance between the two nodes, we see the cut that partitions out node n_1 or n_2 will have a very small value.

In fact, any cut that partitions out individual nodes on the right half will have smaller cut value than the cut that partitions the nodes into the left and right halves.

To avoid this unnatural bias for partitioning out small sets of points, the paper propose a new measure of disassociation between two groups. Instead of looking at the value of total edge weight connecting the two partitions, our measure computes the cut cost as a fraction of the total edge connections to all the nodes in the graph. It's call the normalized cut (Ncut):

$$Ncut(A,B) = \frac{cut(A.B)}{assoc(A,V)} + \frac{cut(A,B)}{assoc(B,V)} \tag{2.2}$$

Where assoc(A,V) is the total connection from nodes in A to all nodes in the graph and assoc(B,V) is similarly defined. With this definition of the disassociation between the groups, the cut that partitions out small isolated points will no longer have small Ncut value, since the cut value will almost certainly be a large percentage of the total connection from that small set to all other nodes.

In the same way, it can define a measure for total normalized association within groups for a given partition:

$$Nassoc(A,B) = \frac{assoc(A,A)}{assoc(A,V)} + \frac{assoc(B,B)}{assoc(B,V)} \tag{2.3}$$

Where assoc(A,A) and assoc(B,B) are total weights of edges connecting nodes within A and B, respectively. We see again this is an unbiased measure, which reflects how tightly on average nodes within the group are connected to each other. Another

important property of this definition of association and disassociation of a partition is that they are naturally related:

$$
\begin{aligned}
Ncut(A,B) &= \frac{cut(A,B)}{assoc(A,V)} + \frac{cut(A.B)}{assoc(B,V)} \\
&= \frac{assoc(A,V) - assoc(A,A)}{assoc(A,V)} + \frac{assoc(B,V) - assoc(B,B)}{assoc(B,V)} \\
&= 2 - \frac{assoc(A,A)}{assoc(A,V)} + \frac{assoc(B,B)}{assoc(B,V)} \\
&= 2 - Nassoc(A,B)
\end{aligned}
\tag{2.4}
$$

Hence, the two partition criteria that we seek in our grouping algorithm, minimizing the disassociation between the groups and maximizing the association within the groups , are in fact identical and can be satisfied simultaneously. In our algorithm, we will use this normalized cut as the partition criterion.

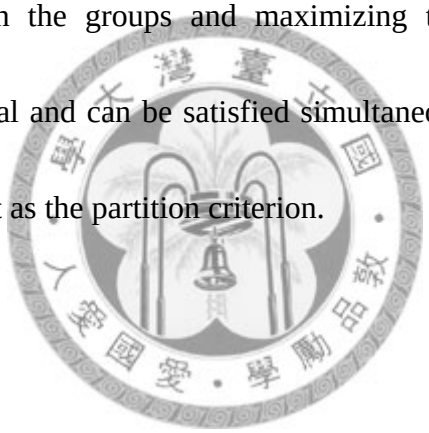

2.2 Gradient Vector Flow

Snakes [25], or active contours, are curves defined within an image domain that can move under the influence of internal forces coming from within the curve itself and external forces computed from the image data. The internal and external forces are defined so that the snake will conform to an object boundary or other desired features within an image. Snakes are widely used in many applications, including edge detection , shape modeling [26-27], segmentation [28-29].

A traditional snake is a curve, that moves through the spatial domain of an image to minimize the energy functional:

$$E = \int_0^1 \frac{1}{2}\left[\alpha \left| x'(s) \right|^2 + \beta \left| x''(s) \right|^2 \right] + E_{ext}\left(x(s) \right) ds \tag{2.5}$$

The external energy function E_{ext} is derived from the image so that it takes on its smaller values at the features of interest, such as boundaries. Given a gray-level image I(x,y) , viewed as a function of continuous position variables (x,y), typical external energies designed to lead an active contour toward step edges are:

$$\begin{aligned} E_{ext}^{(1)}(x,y) &= -\left| \nabla I(x,y) \right|^2 \\ E_{ext}^{(2)}(x,y) &= -\left| \nabla \left[G_\sigma(x,y) * I(x,y) \right] \right|^2 \end{aligned} \tag{2.6}$$

where G_σ(x,y)is a two-dimensional Gaussian function with standard deviation and gradient operator. If the image is a line drawing (black on white), then appropriate external energies include

$$E_{ext}^{(3)}(x,y) = I(x,y)$$
$$E_{ext}^{(4)}(x,y) = G_{\sigma}(x,y) * I(x,y) \tag{2.7}$$

A snake that minimizes E must satisfy the Euler equation :

$$\alpha x''(s) - \beta x''''(s) - \nabla E_{ext} = 0 \tag{2.8}$$

This can be viewed as a force balance equation

$$F_{\text{int}} + F_{ext}^{(p)} = 0 \tag{2.9}$$

The internal force discourages stretching and bending while the external potential force pulls the snake toward the desired image edges. The gradient vector flow snake approach is to use the force balance condition as a starting point for designing a snake. It define below a new static external force field, which we call the gradient vector flow (GVF) field. To obtain the corresponding dynamic snake equation, we replace the potential force, yielding :

$$x_t(s,t) = \alpha x''(s,t) - \beta x''''(s,t) + v \tag{2.10}$$

We call the parametric curve solving the above dynamic equation a GVF snake. It is solved numerically by discretization and iteration, in identical fashion to the traditional snake. Although the final configuration of a GVF snake will satisfy the force-balance equation, this equation does not, in general, represent the Euler equations of the energy minimization problem. This is because v(x,y) will not, in general, be an irrotational field . The loss of this optimality property, however, is well-compensated by the significantly improved performance of the GVF snake.

We define the gradient vector flow field V(x,y) = [u(x,y) , v(x,y)] to be the vector field that minimizes the energy functional

$$\begin{aligned} \mu\nabla^2 u - (u - f_x)\left(f_x^{\,2} + f_y^{\,2}\right) = 0 \\ \mu\nabla^2 v - (v - f_y)\left(f_x^{\,2} + f_y^{\,2}\right) = 0 \end{aligned} \tag{2.11}$$

This variational formulation follows a standard principle, that of making the result smooth when there is no data. In particular, we see that when $|\nabla f|$ is small, the energy is dominated by sum of the squares of the partial derivatives of the vector field, yielding a slowly varying field. On the other hand, when $|\nabla f|$ is large, the second term dominates the integrand, and is minimized by setting v = ∇f . This produces the desired effect of keeping v nearly equal to the gradient of the edge map when it is large, but forcing the field to be slowly-varying in homogeneous regions.

The parameter μ is a regularization parameter governing the tradeoff between the first term and the second term in the integrand. This parameter should be set according to the amount of noise present in the image.

We note that the smoothing term —the first term within the integrand by Horn and Schunck in their classical formulation of optical flow [30]. It has recently been shown that this term corresponds to an equal penalty on the divergence and curl of the vector field [31]. Therefore, the vector field resulting from this minimization can be expected to be neither entirely irrotational nor entirely solenoidal.

Using the calculus of variations [32], it can be shown that the GVF field can be

found by solving the following Euler equations :

$$\begin{aligned} \mu\nabla^2 u - (u - f_x)\left(f_x^{\,2} + f_y^{\,2}\right) = 0 \\ \mu\nabla^2 v - (v - f_y)\left(f_x^{\,2} + f_y^{\,2}\right) = 0 \end{aligned} \tag{2.12}$$

These equations provide further intuition behind the GVF formulation. We note that in a homogeneous region, the second term in each equation is zero because the gradient of f(x,y) is zero. Therefore, within such a region, and are each determined by Laplace's equation, and the resulting GVF field is interpolated from the region's boundary, reflecting a kind of competition among the boundary vectors [33].

Chapter 3 Method

3.1 Clinical Experiment

The image raw data is gathered by Dr.Chang in National Taiwan University Hospital. This clinical experiment is performance in 1.5T Siemens MRI system. We use gadolinium as contrast agent and Avastin as the chemotherapy drugs.

After inject the contrast agent, we scan the patient's lung 100 frames in about 100 seconds, each frame will have four sagittal view images and one axial view image.

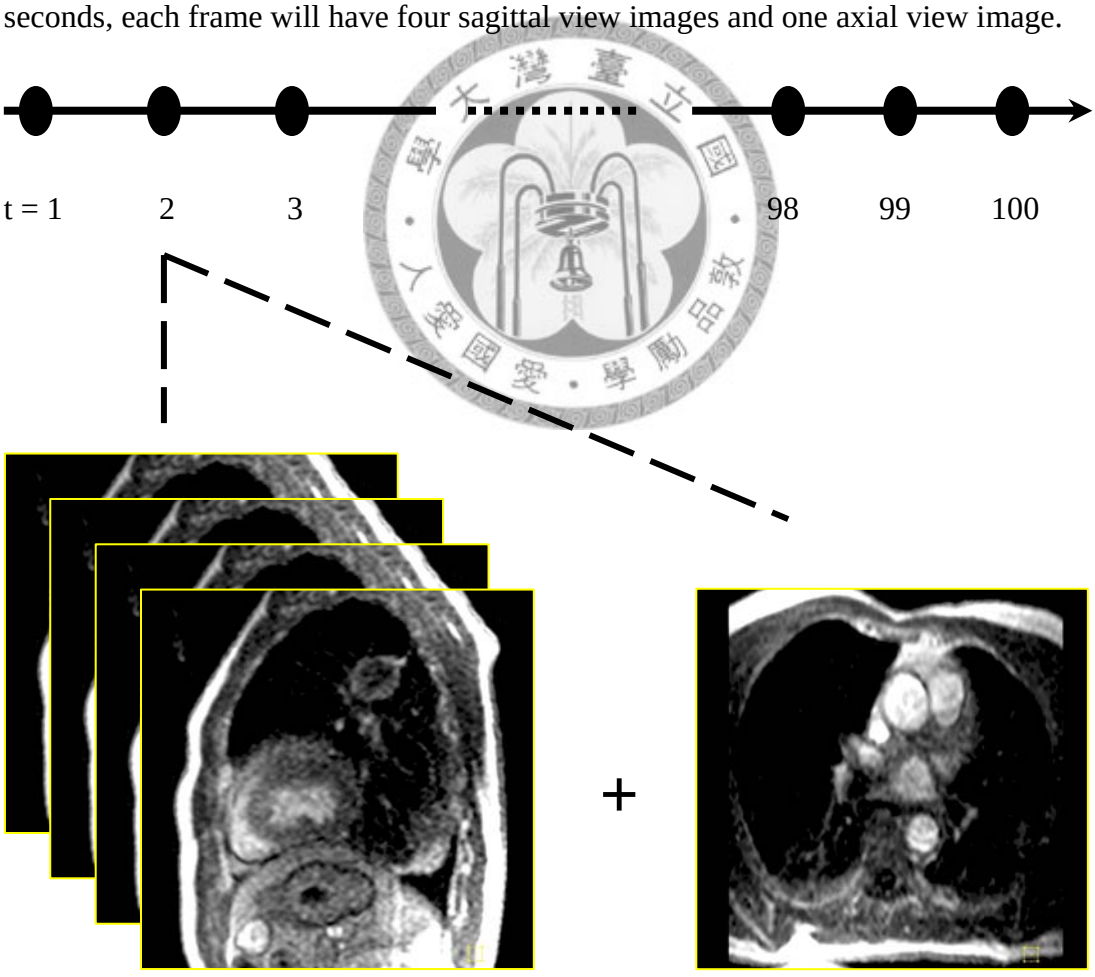

Fig 3.1 Image sequence in the clinical experiment.

3.2 Pre-processing in DICOM images

After DCE-MRI experiments, the console will output DICOM format images. If we want avoid motion effect in Mistar software, we should do motion correct operation before the DICOM input to the Mistar software.

Suppose we have two images like figure 3.2. Left side is the reference image (we suppose the tumor position is correct), and right side is temporal image (the tumor position will have shift effect because of the motion during scan process) which we want to correct it.

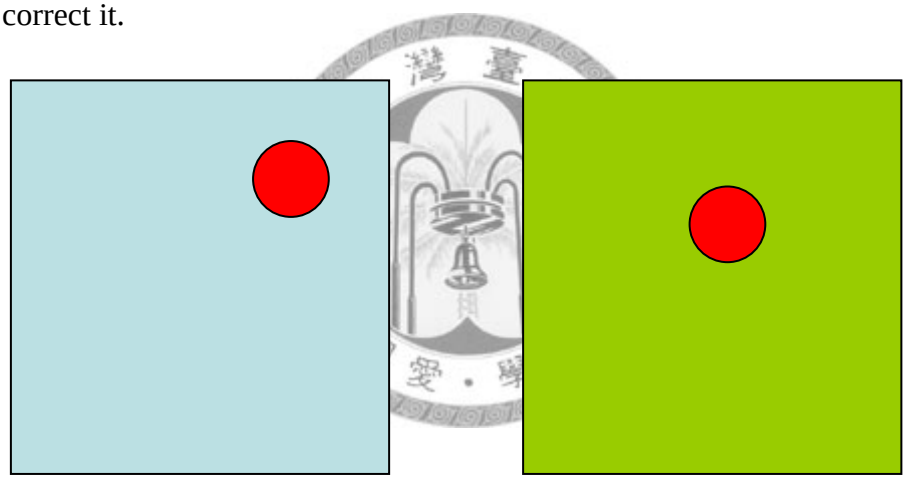

Reference Image Temporal Image

Figure 3.2 Reference image and temporal image.

The red circle indicate the tumor (to simplify the motion problem, we assume the tumor volume in each image is the same with each other), and we can clearly identify the tumor position (red circle) in reference image and temporal image is quite different. If we input the sequence DICOM image data to the Mistar software, we supposed it will have incorrect calculated information like figure 3.3.

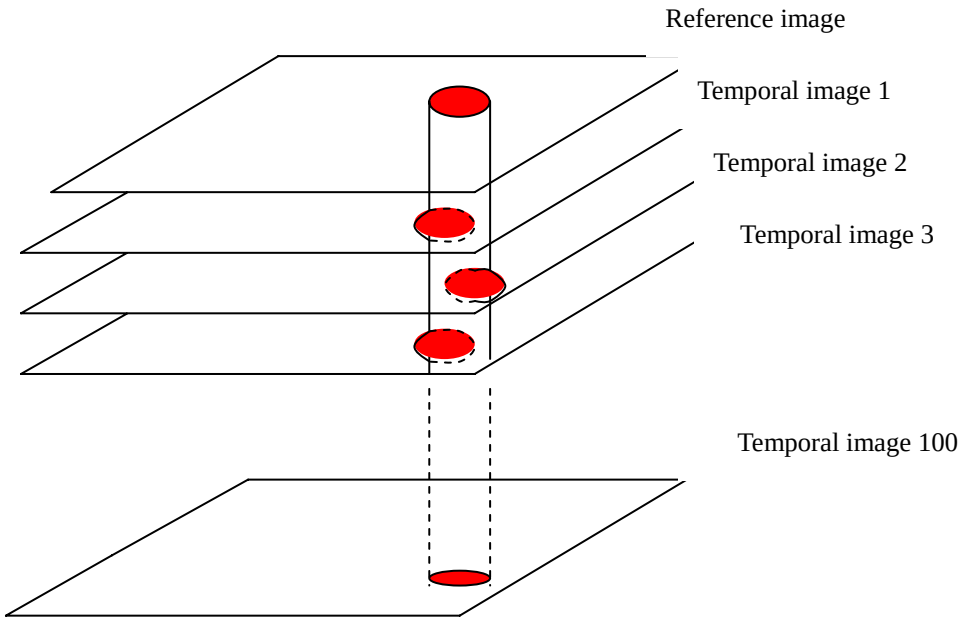

Figure 3.3 Registration problem in sequential images.

To solve this problem, we using correlation method in image registration. For example, if we have two images like figure 3.2. The goal is that we want to put tumor in both images in the same position (fig 3.4).

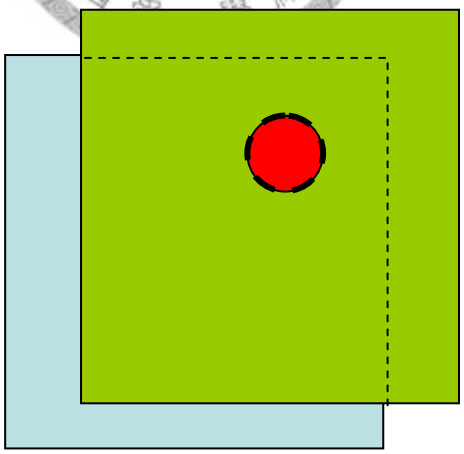

Figure 3.4 Adjust motion problem by moving temporal image to reference image.

In fact, we select reference image in first time. Then we will find out the proper ROI in reference image (Fig 3.5) making the correlation with temporal images.

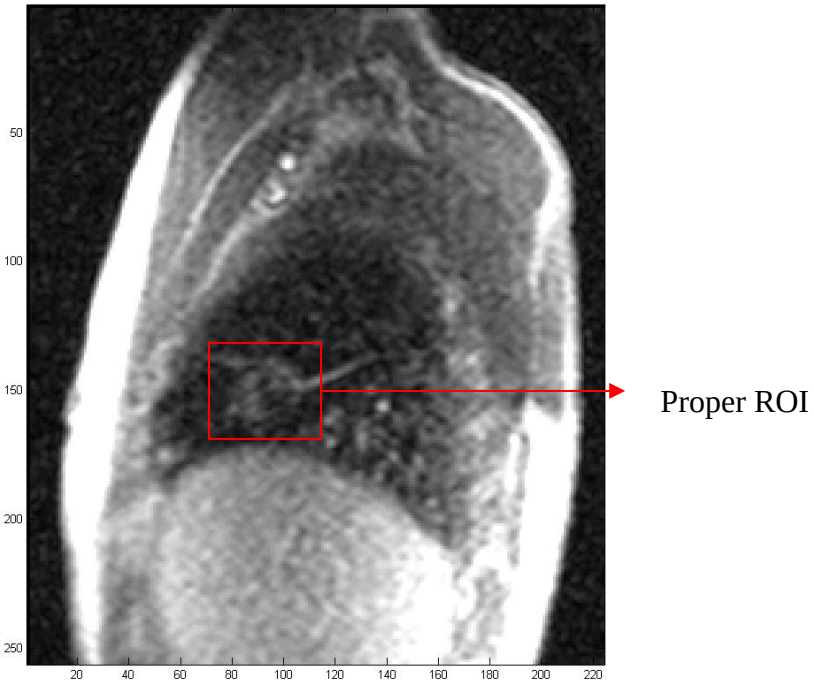

Fig 3.5 Select proper ROI in reference image.

We will get the proper ROI from the reference image to compare with the similar area in the temporal images (Fig 3.6)

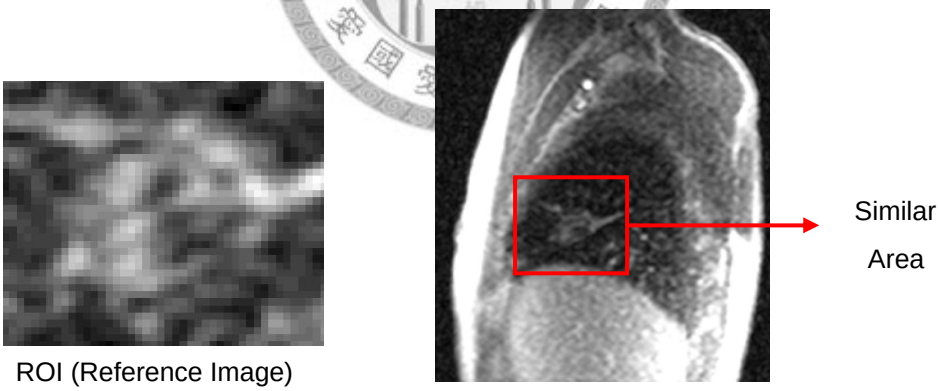

Fig 3.6 Get proper ROI from the reference image to compare with the similar area in the temporal images.

To increase the specification in tumor property, we can select the tumor position by user defined or by automatic segmentation method.

By User defined

Step 1: Select the contour by user (dot line) in Fig 3.7

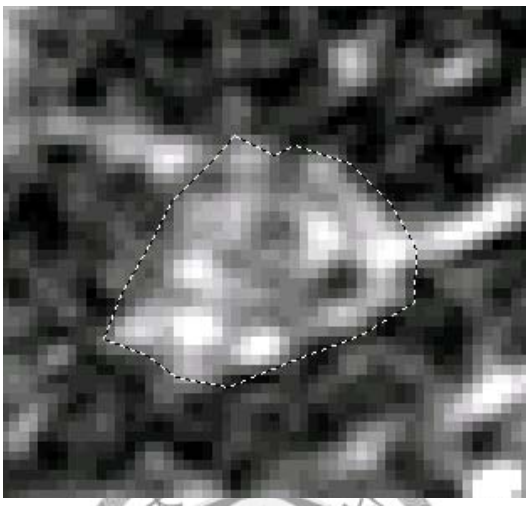

Fig 3.7 Contour which decided by user.

Step 2: We set gray level in the area outside the contour be zero (black) in Fig 3.8

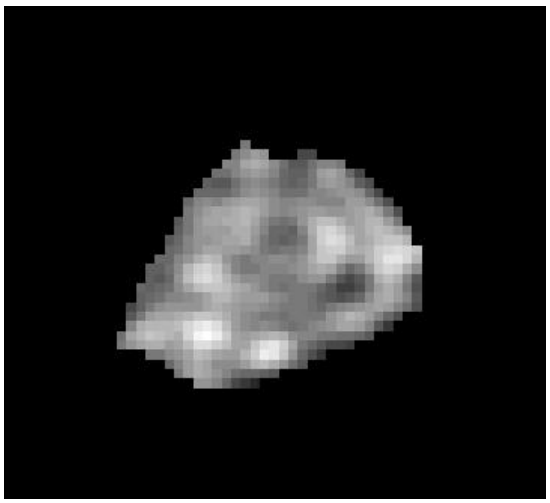

Fig 3.8 Make outside gray level be zero.

By automatic segmentation method

Step 1: Select the area which normalize cut will do operation in Fig 3.9

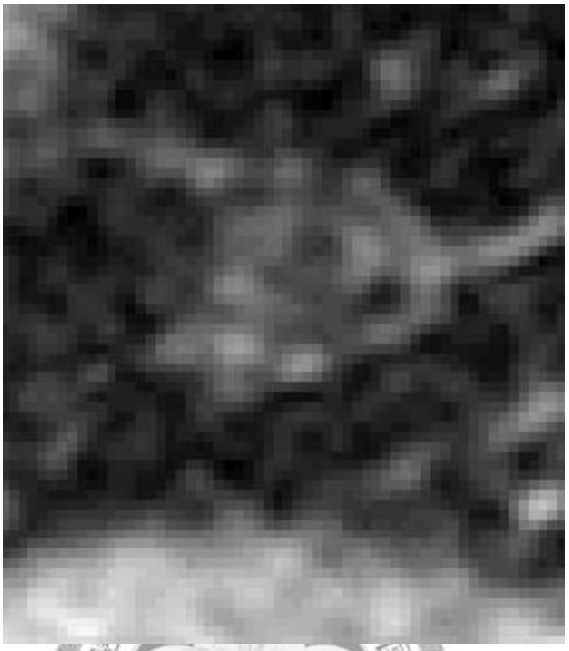

Fig 3.9 Prepare proper ROI for normalize cut.

Step 2: After running normalize cut program, we get a binary image and its corresponding gray level image in Fig 3.10.

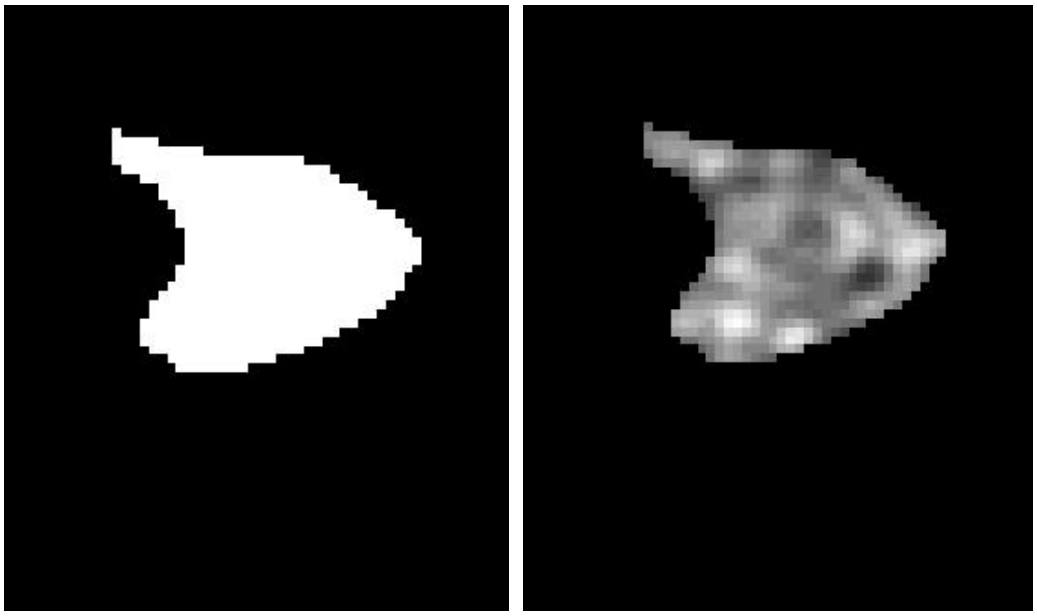

Fig 3.10 Results which determined by the normalize cut operation.

Step 3: Run the gradient vector flow (GVF) program to determined the contour in Fig 3.11 ~ Fig 3.13

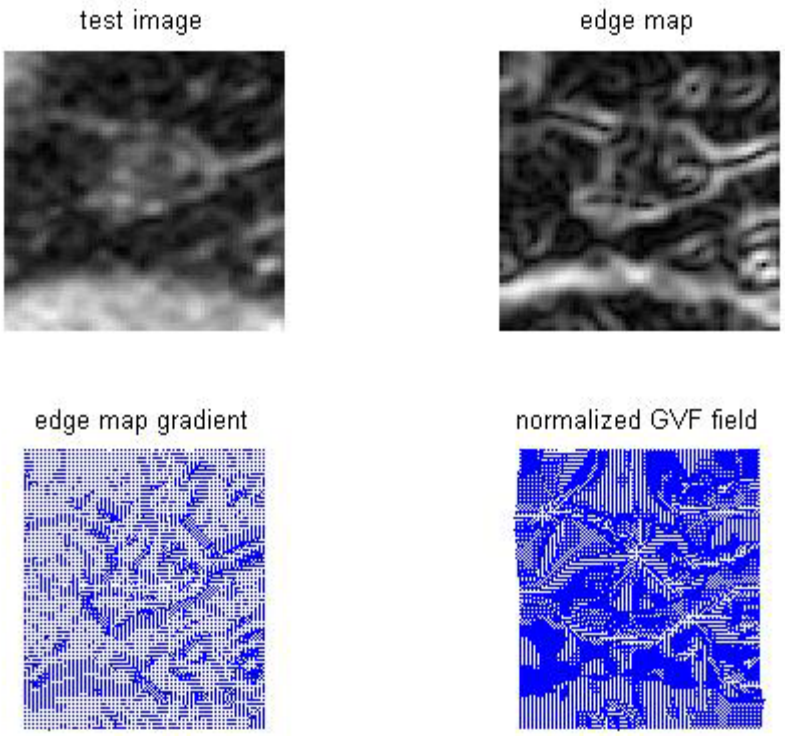

Fig 3.11 Four maps (test image, edge map, edge map gradient, normalized GVF field) for determined gradient vector flow.

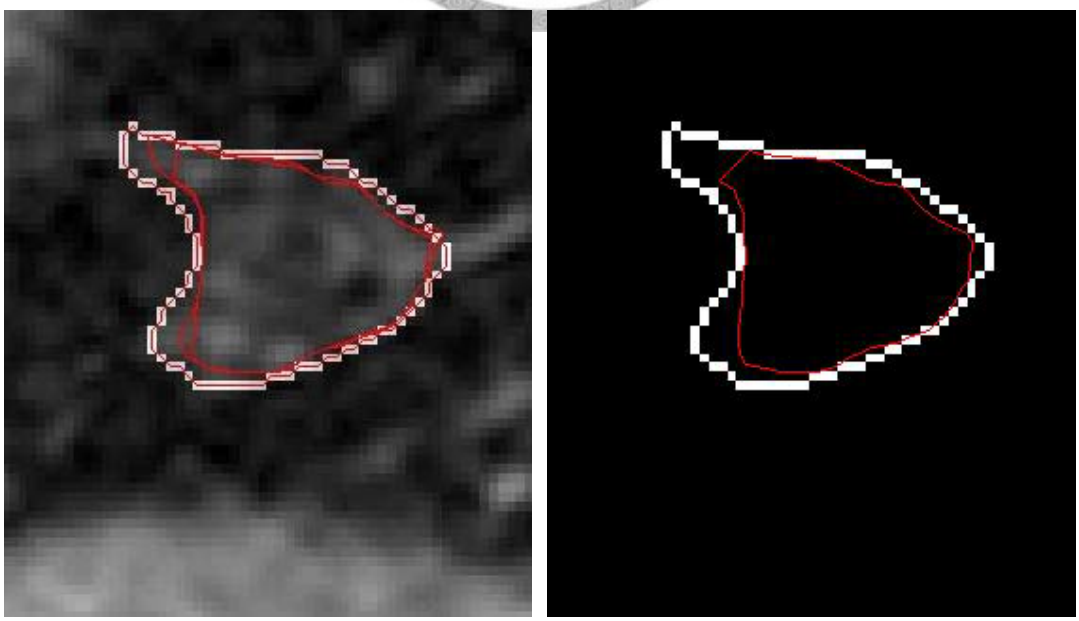

Fig 3.12 Running gradient vector flow program to determined the contour

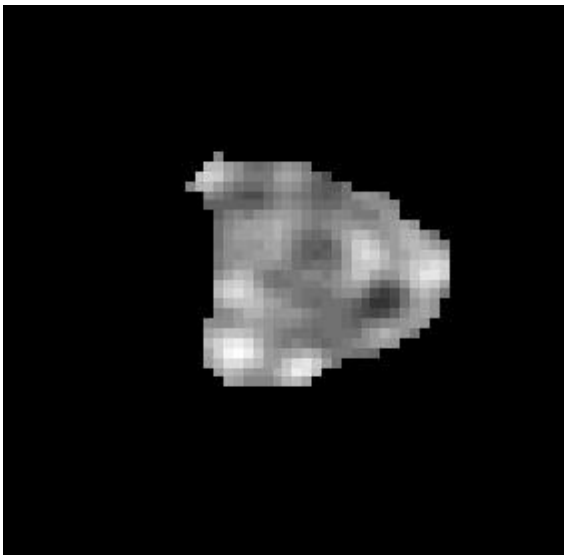

Fig 3.13 Final image which decided by normalize cut and gradient vector flow.

The similar area should be the possible area which tumor position is inside in the temporal images. Although the tumor position in temporal images is differ with each other, the tumor position in reference image will provide a standard to deal with the problem. Since we already get the ROI in both reference image and temporal image, the maximum correlation will determined the correct position.

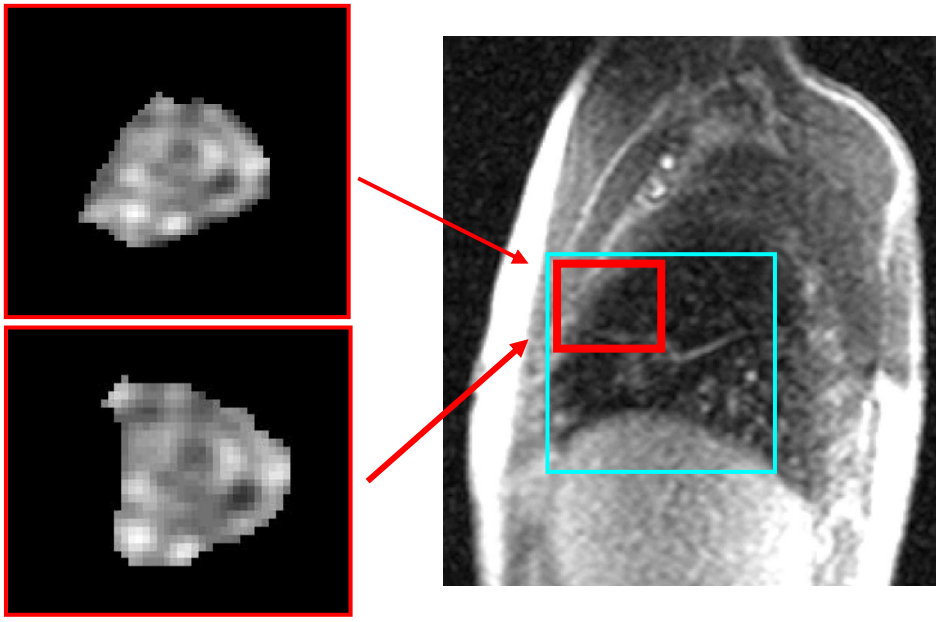

Fig 3.14 Correlation between reference and temporal image

After we do the correlation with the reference and temporal image, there exist many correlation coefficients. What we want is the maximum correlation coefficient.

The maximum correlation coefficient represent the most proper tumor position in the temporal images. Once we find the proper position, the next step is to shift the temporal images to the new position (fig3.8).

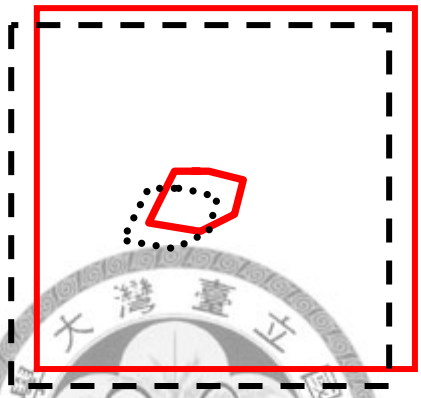

Fig 3.15 Shift temporal images to the arbitrarily position which correlation value is maximum.

Since we suppose the tumor is rigid, the reference image will change to get the most similarity in tumor shape. That is, the image which was corrected will be the next reference image. Under the assumption, we suppose to correct total temporal images in the whole image sequences.

3.3 Mistar software processing

We use the commercial software Mistar to accomplish the DCE-MRI study and identify the difference between image data with motion correct or not.

After we lunch the DICOM data from MRI console, it shows the lung image in both sagittal and axial view in the upper right during the software window. In order to find the arterial input function (AIF), we select the axial view and set the ROI (yellow square) in the aorta to get the AIF. The upper right shows the 100 time frames signal intensity in aorta which used to be the AIF.

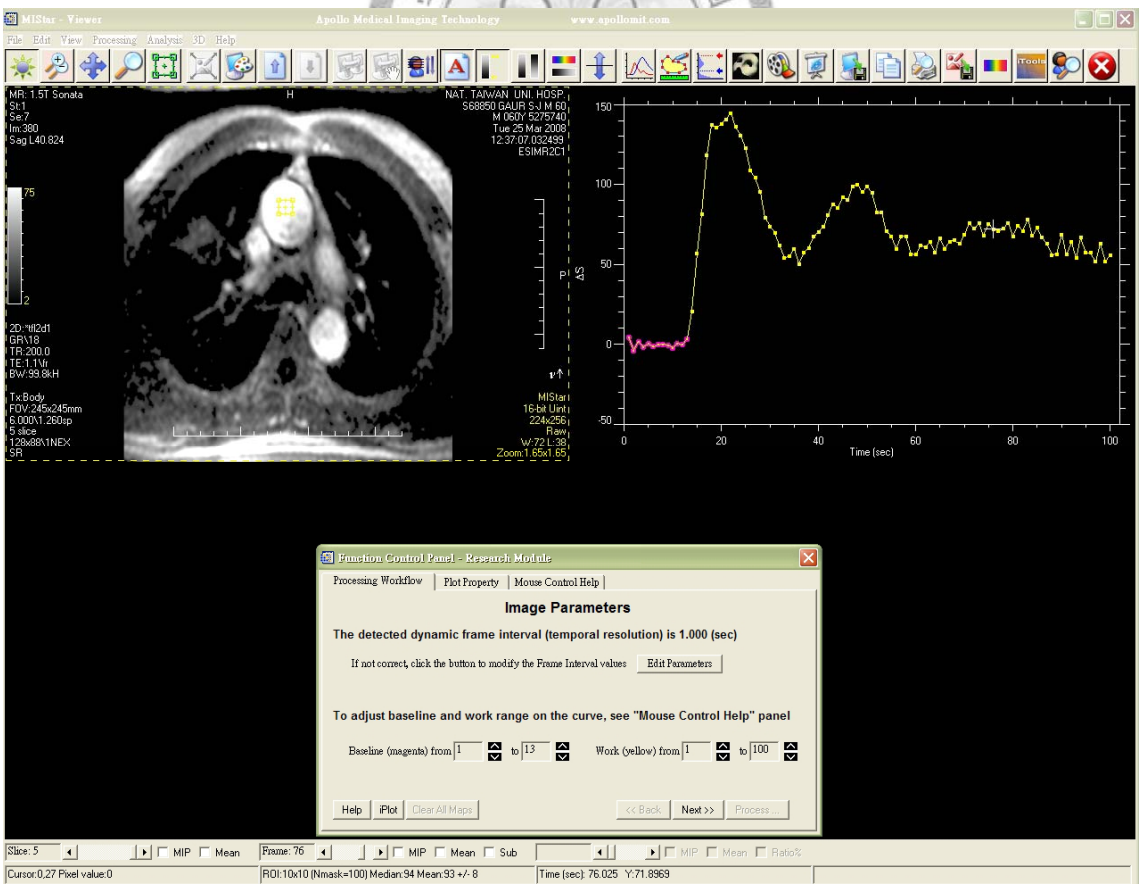

Fig 3.16 Interface in operating Mistar software.

Besides select the AIF, we also decided the area which need to be calculated in the software. The selection of the area should be include the tumor and not exceed to much to waste the processing time (fig 3.17).

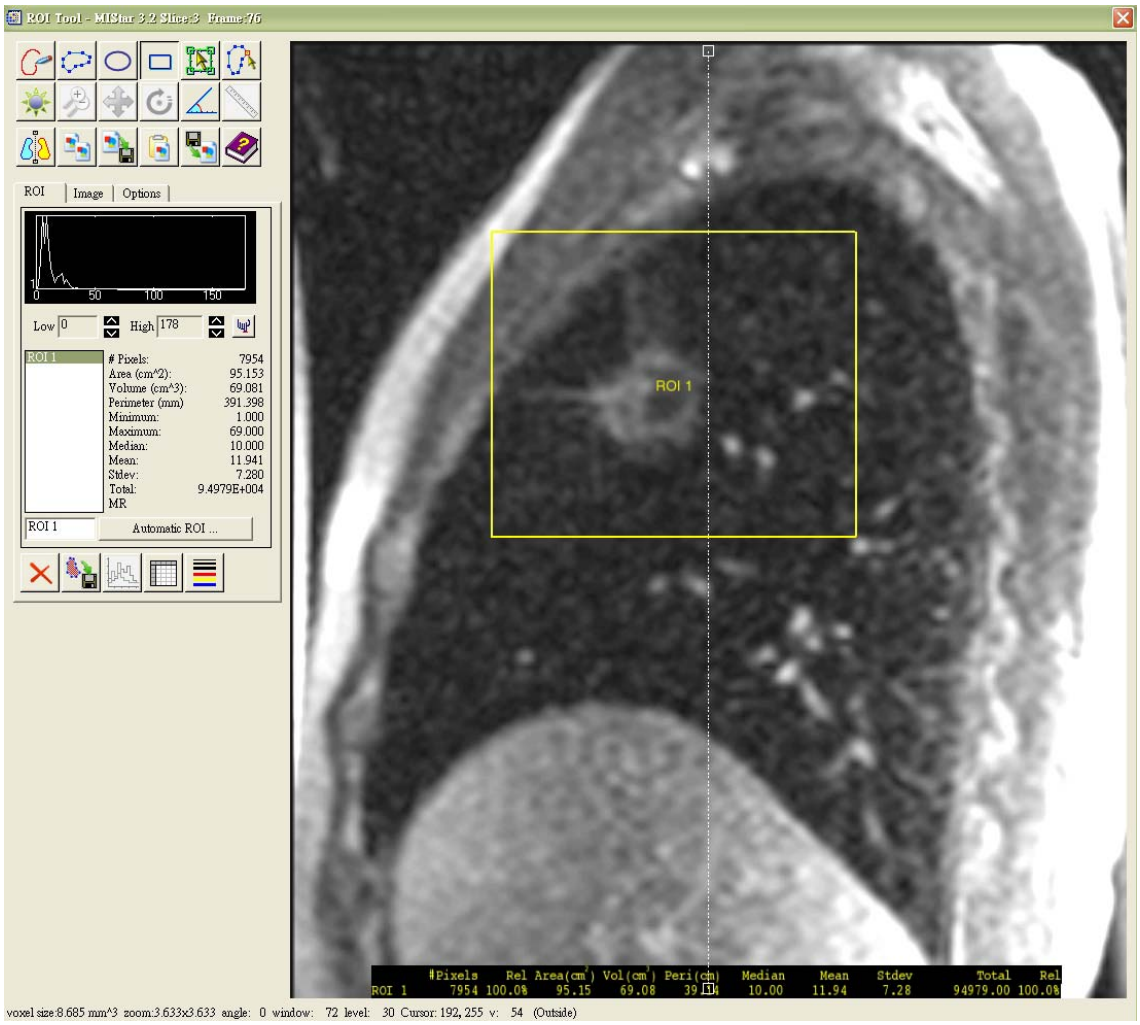

Fig 3.17 Select processing area to in Mistar software. If we select large area, it will spend more time to finish the calculation.

When we decided the curve of AIF and the region which needed to be execute, then we can push the processing button to run the entire calculation like fig 3.18.

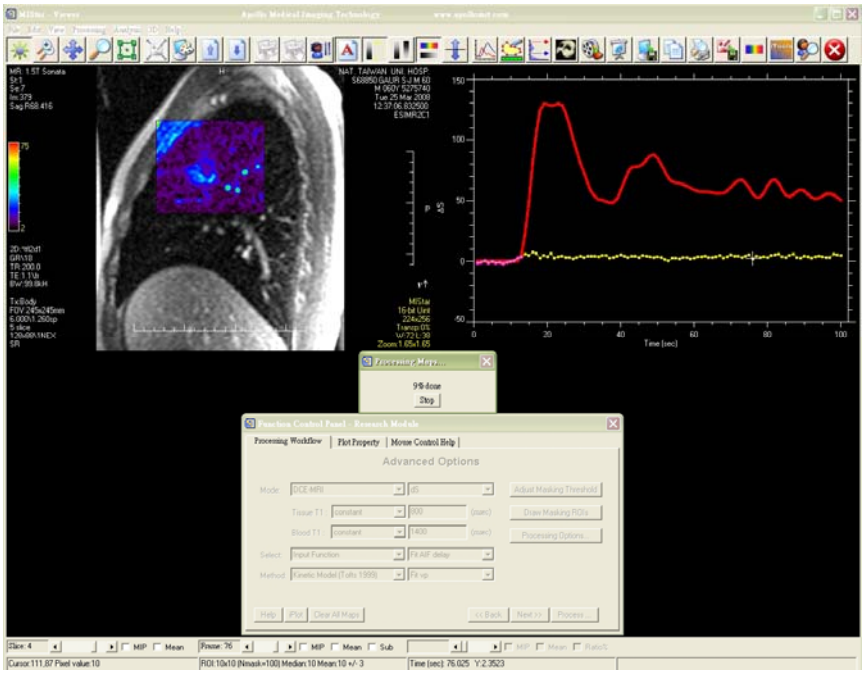

Fig 3.18 Processing the calculation (blue image is the area which selected to calculate).

After Processing, we can get the DCE-MRI parameter maps . For example: The Upper left is k_{ep}; the upper right is V_e; the lower left is K^{trans}; the lower right is V_p.

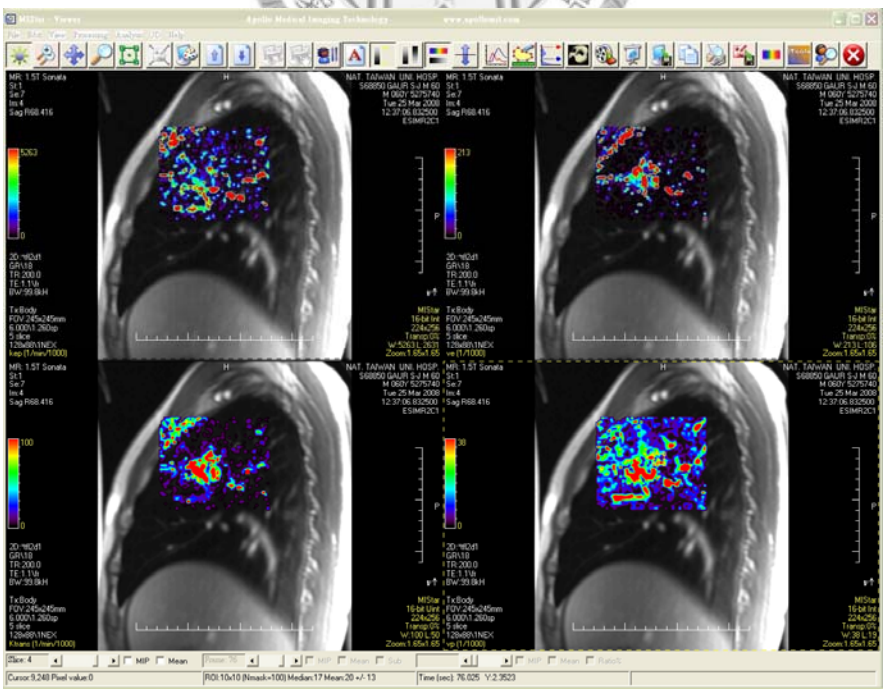

Fig 3.19 DCE-MRI parameter maps (upper right is v_e, upper left is k_{ep}, lower right is v_p, and lower left is k^{trans}).

Chapter 4 Results

4.1 Results from Mistar software

After we finish the processing in Mistar software, the parameter maps will show us the information about the DCE-MRI.

First, we should select the most proper tumor contour in the maps. We can console the T1-contrast image for reference to adjust the correct contour (fig 4.1).

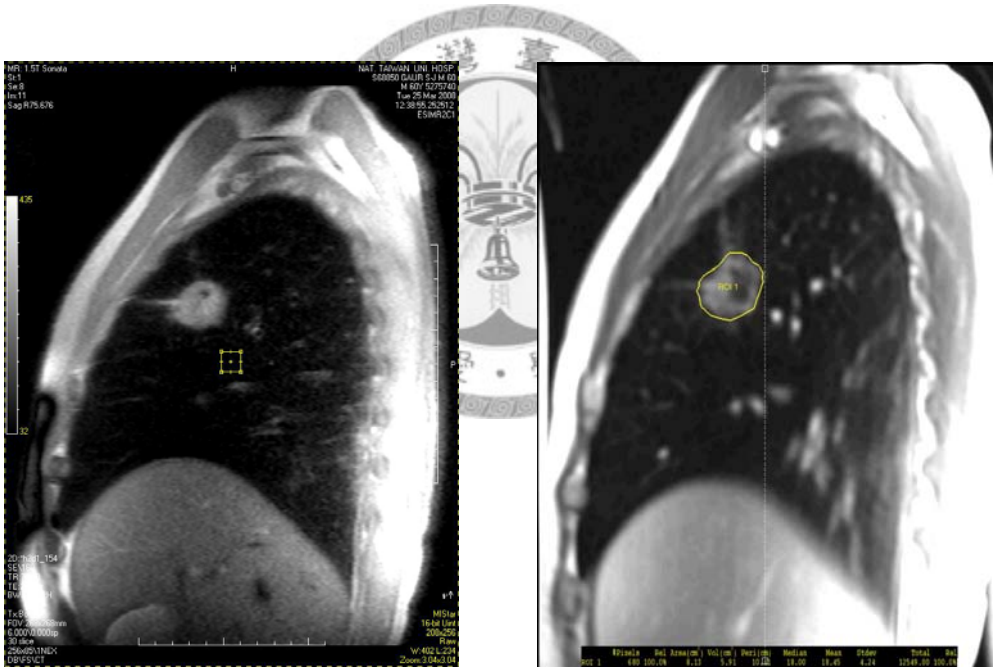

T1-Contrast enhance Image T1-Weighted Image

Fig 4.1 Select tumor contour by doctor to make sure the area is exactly in tumor position.

When we select the proper contour about the tumor, the DEC-MEI parameter maps can be also determinate like the fig 4.2.

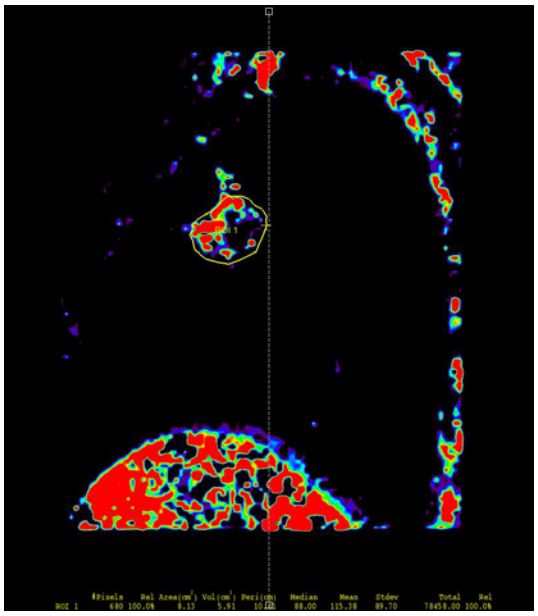

K^{trans} Map

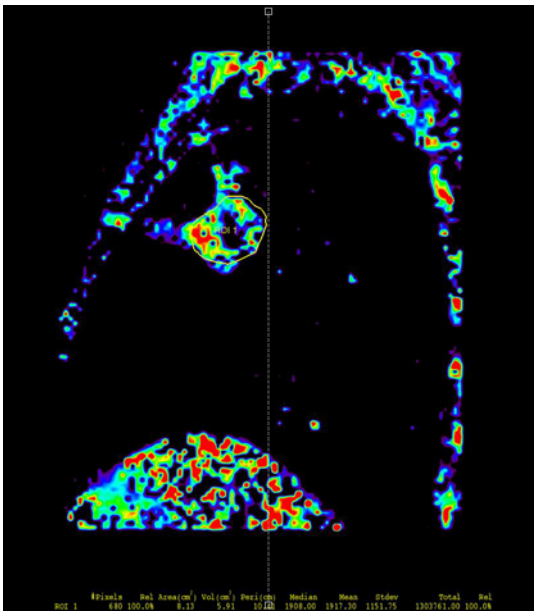

K_{ep} Map

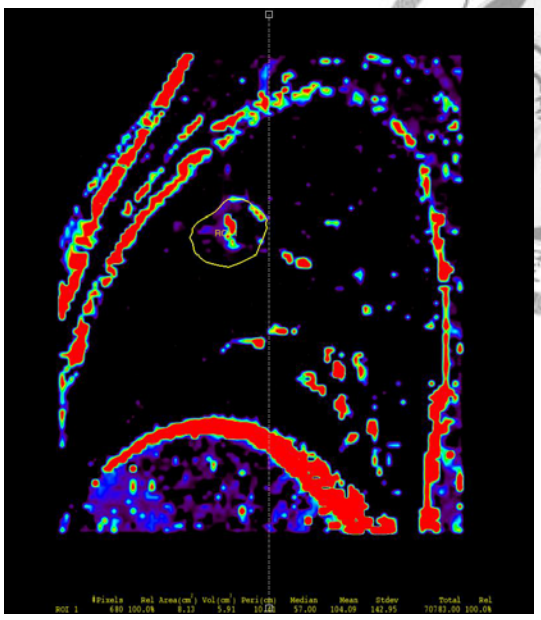

V_e Map

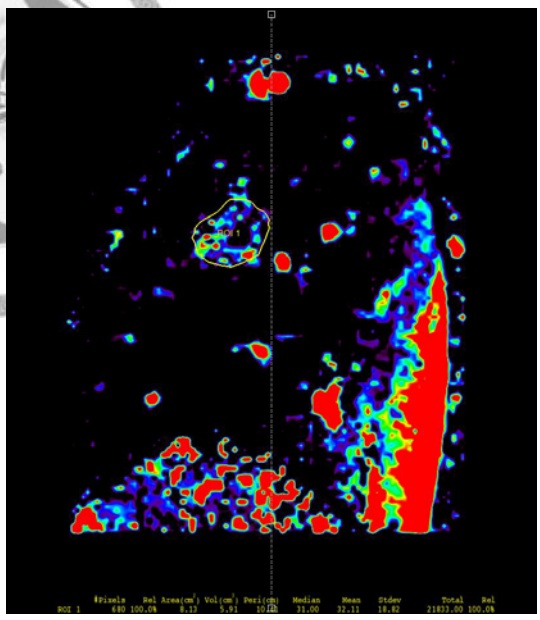

V_p Maps

Fig 4.2 Four parameters maps results which calculated by Mistar software, the yellow line in the pictures are the tumor position and shape decided by doctor.

The Mistar software allows us to output the detail values in each pixel which is in the range of tumor contour. Because we want to know the information in entire tumor,

we should calculate the values in all slices. Here we have four slices in the sagittal view, and there should be four different parameter maps ex: K^{trans}.

The following table shows the data which we collect in this experiment. There are eleven patients in it. Some of them having twice or three times cases, even four times is include.

Chart No.	Age	Gender		date of MRI	K^{trans} (mean)	K^{trans} (SD)	K_{ep} (mean)	K_{ep} (SD)	V_e (mean)	V_e (SD)	V_p (mean)	V_p (SD)	Pixel Np.	Volume
F779	52	F	before	20080110	172.8782	86.5904	1263	511.1793	146.4887	69.9464	38.0406	22.3202	3792	26.24
			after		156.4238	119.044	1355	1439	273.98	421.8603	46.7213	35.2522		
			before	20080131	127.1347	77.6199	1299	669.2082	110.8461	84.0982	31.8774	31.1185	3735	25.87
			after		114.408	86.1253	1268	871.3224	123.993	136.2469	35.5293	31.9941		
			before	20080220	110.3947	48.4889	969.2542	502.518	164.1305	126.0281	24.6484	16.2942	2085	14.44
			after		122.5904	51.9391	996.4077	492.7662	166.7213	120.7124	24.142	16.7437		
M329	62	M	before	20070526	98.0442	95.8564	1164	1004	101.6869	118.3307	23.3014	23.8693	10241	76.69
			after		90.019	92.0413	1024	949.2185	116.109	150.226	23.5816	23.6555		
			before	20070801	44.4853	55.767	710.7123	1003	122.2082	199.0388	29.1401	29.3651	4731	38.2
			after		34.1365	60.8422	457.9362	936.201	165.4887	284.2617	24.7339	29.3889		
			before	20071003	57.8705	73.7613	850.1242	1062	83.4321	121.6247	21.1146	25.1096	2826	28.18
			after		45.9646	86.4798	742.3719	1526	74.1359	163.2148	25.9409	33.4157		
			before	20071121	45.1077	54.8354	822.802	922.8821	56.2496	75.8963	21.0384	21.8096	5025	43.64
			after		47.6603	59.579	721.9954	923.8309	85.7731	139.319	22.7389	27.2716		
M871	49	M	before	20080118	96.9632	57.9461	1636	879.2621	83.6799	92.9254	31.7942	20.1439	4155	36.09
			after		93.7745	67.0807	1544	1006	98.8046	113.8152	33.3875	22.6192		
			before	20080212	52.9786	43.0451	1014	813.8075	92.4277	113.5992	23.4994	21.2353	2429	21.09
			after		59.7205	61.7942	1128	888.0041	77.1618	83.8275	21.4063	19.161		

Chart No.	Age	Gender		date of MRI	K^{trans} (mean)	K^{trans} (SD)	K_{ep} (mean)	K_{ep} (SD)	V_e (mean)	V_e (SD)	V_p (mean)	V_p (SD)	Pixel Np.	Volume
M141	68	M	before	20070529	100.9661	60.5172	781.2155	519.3872	214.7719	197.9482	17.6092	14.2926	3424	23.71
			after		97.9588	57.7668	787.2339	567.8119	229.6203	209.1	20.4229	16.4177		
			before	20070815	87.1577	70.3808	1225	858.1167	89.4633	92.6278	20.2625	17.9677	2042	14.13
			after		81.0984	70.6965	1037	825.8859	122.3457	144.6699	20.1102	18.1868		
			before	20071031	99.6389	85.1381	1175	869.0652	119.4608	104.4188	21.06	18.8583	983	7.94
			after		74.6541	65.4323	870.0458	794.2426	167.2279	234.8201	23.5371	28.6724		
M740	60	M	before	20080325	111.5457	86.375	1948	1276	93.0266	123.4674	34.8995	23.8812	1840	15.97
			after		88.8685	86.7014	1623	1569	198.7152	287.2727	41.1228	28.7461		
			before	20080421	107.3975	56.2021	1639	762.2981	80.0312	66.3173	20.6098	15.1292	961	9.58
			after		93.5109	52.6339	1620	1038	72.6608	77.4495	23.7804	19.9829		
			before	20080509	76.3165	48.3744	1164	779.1787	108.6878	120.3225	16.566	11.9694	1166	11.63
			after		72.7015	67.1446	1089	1382	171.6475	299.9304	16.8148	17.546		
M826	58	M	before	20080402	121.7588	105.2475	1279	862.7111	122.5373	104.345	31.1425	28.5017	10228	70.82
			after		120.7957	119.5485	1206	979.0496	148.0378	184.8912	33.3206	32.2619		
			before	20080429	233.9865	217.0597	1574	983.4117	160.6663	106.3205	49.0664	38.8932	7993	55.34
			after		232.8203	241.7068	1453	1143	306.2463	460.7253	56.6718	56.2376		
			before	20080520	67.4415	63.5726	660.581	545.4191	186.8765	159.4787	23.2834	22.3548	4704	32.56
			after		95.6312	121.7479	958.7119	985.875	222.0485	266.6306	27.6603	26.8991		

Chart No.	Age	Gender		date of MRI	K^{trans} (mean)	K^{trans} (SD)	K_{ep} (mean)	K_{ep} (SD)	V_e (mean)	V_e (SD)	V_p (mean)	V_p (SD)	Pixel Np.	Volume
M469	77	M	before	20061030	219.3056	167.3221	1625	934.4481	128.5896	90.6103	58.9645	40.7381	5275	52.6
			after		194.4157	170.0952	1393	1150	164.4108	203.3105	60.8883	47.0387		
			before	20061205	40.5627	44.0976	680.6431	781.0105	85.153	136.4305	33.1725	31.6663	3444	34.34
			after		45.6771	58.8942	645.5044	835.5118	76.261	118.7002	27.6519	29.4886		
			before	20070111	89.1366	100.7679	794.7162	801.439	146.5321	202.2965	45.5301	43.4019	5591	38.62
			after		80.3615	112.4534	722.1975	922.8178	136.6053	208.5487	48.299	50.8263		
F928	58	F	before	20080119	238.59	123.8953	2185	863.2497	115.288	49.7335	55.4066	29.0878	7765	53.75
			after		226.4178	138.2651	1881	1122	217.97	305.2919	66.1131	39.5759		
			before	20080214	89.6262	61.2078	1545	809.7152	76.6474	70.779	44.6246	21.4567	6817	47.19
			after		51.7822	45.7289	1079	1003	88.0855	127.0202	53.5089	29.2859		
			before	20080306	106.0227	48.1355	1542	633.4481	79.243	41.985	35.8371	16.0028	749	5.18
			after		109.0774	57.4687	1311	690.5937	134.7704	136.7922	37.5701	18.058		
M372	41	M	before	20070602	205.999	98.3014	2052	978.0806	116.5311	75.6308	37.5079	23.2589	3099	21.46
			after		180.6705	104.3126	1672	1016	153.9742	148.2009	40.5608	32.3914		
			before	20070816	81.0472	42.49	1073	634.5683	106.9744	90.8074	21.0072	14.3647	1249	8.65
			after		80.5124	42.4462	1002	683.3029	131.9744	128.8156	22.1954	15.6253		

Chart No.	Age	Gender		date of MRI	K^{trans} (mean)	K^{trans} (SD)	K_{ep} (mean)	K_{ep} (SD)	V_e (mean)	V_e (SD)	V_p (mean)	V_p (SD)	Pixel Np.	Volume
M664	47	M	before	20070801	69.9793	44.6357	1133	754.1266	113.6001	125.8711	26.2577	19.9017	1688	11.68
			after		53.2725	41.0073	853.5101	795.0104	145.8181	195.008	30.8104	23.3339		
			before	20071003	35.2455	43.9684	700.7417	796.9888	60.7749	83.7166	32.3862	22.407	1173	8.11
			after		28.7025	39.6834	424.3495	632.6747	91.1705	154.0047	35.1117	25.7059		
M807	44	M	before	20070725	178.2295	145.7388	1810	1176	130.5924	123.2023	92.6686	45.5533	1521	13.21
			after		142.2906	146.8902	1538	1629	123.5095	134.204	98.4313	56.2298		
			before	20071011	81.6464	54.1193	1231	795.6572	112.3391	109.3154	31.6754	15.0083	345	3.45
			after		70.7594	56.9641	1028	917.3103	162.9246	233.9392	36.3101	22.3327		

Table 4.1 Four parameter values in each patient include the mean and standard deviation.

4.2 Data analysis

The common catalog about the cancer chemotherapy treatment can be divided into three terms: Before (Baseline) treatment, Immediate after treatment (after the first course of chemotherapy) and final treatment (the final study before stopping chemo-therapy).

We divided the patient into two groups. Group A: The treatment include only before treatment and final treatment; Group B: the treatment include before treatment, immediate after treatment and final treatment. We can plot the histogram about the four DCE-MRI parameters to comment the response of treatment.

The following figure shows these parameters which the patient in group A. The vertical axis shows the normalize of the number of pixels in the area which we consider is tumor, while the horizontal axis means the normalized histograms of amplitude in each DCE-MRI parameters (K^{trans},K_{ep},Ve,Vp).

Group A (M372)

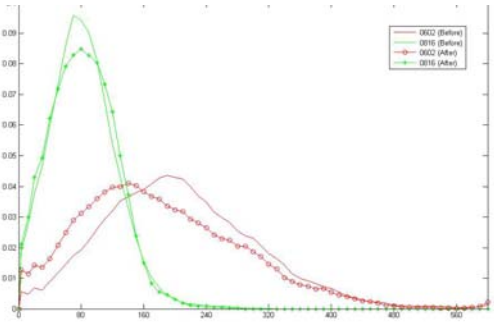

K^{trans}

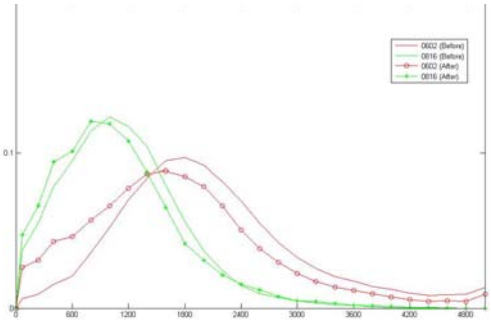

K_{ep}

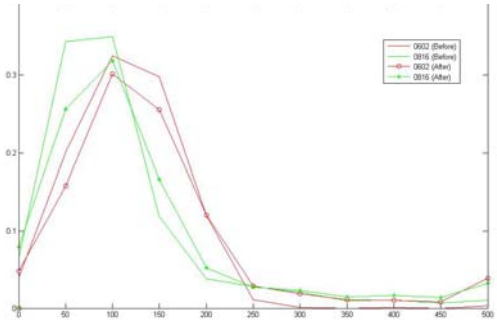

V_e

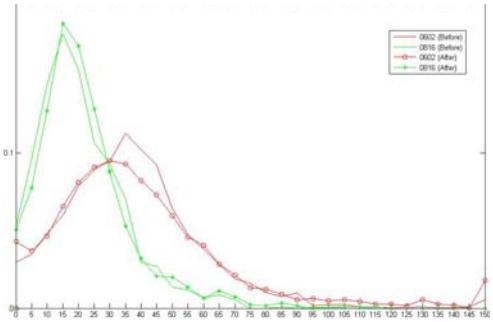

V_p

Group A (M807)

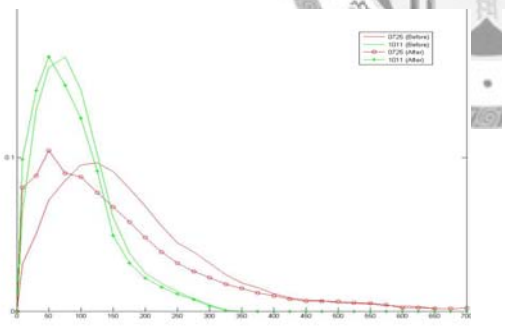

K^{trans}

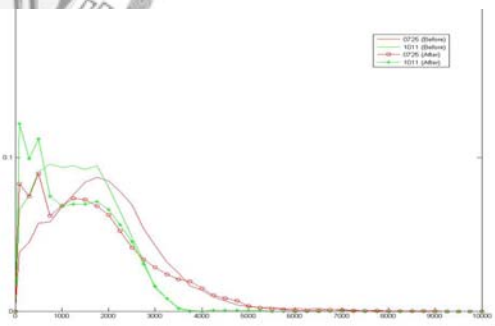

K_{ep}

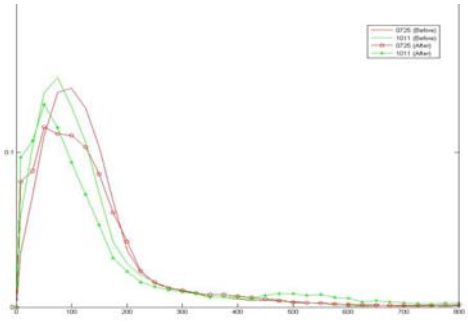

V_e

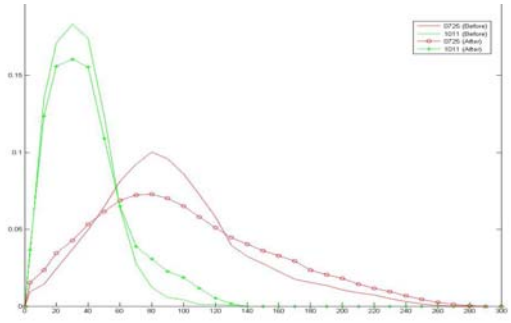

V_p

Group A (M664)

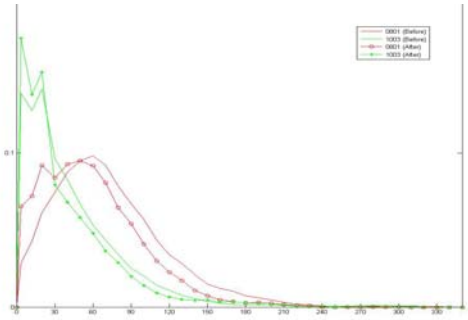

K^{trans}

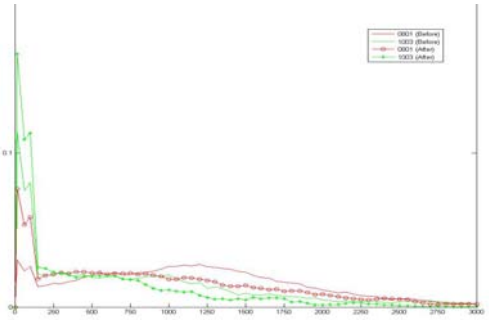

K_{ep}

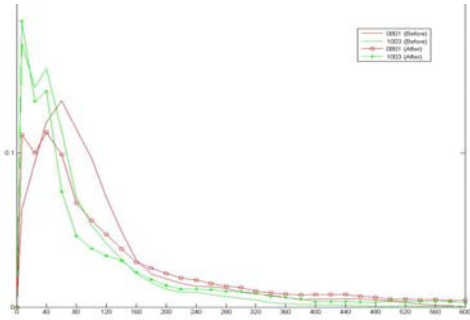

V_e

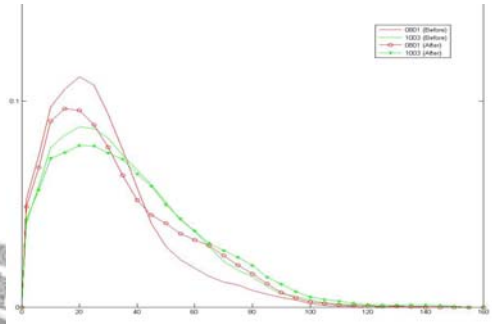

V_p

Group A (M871)

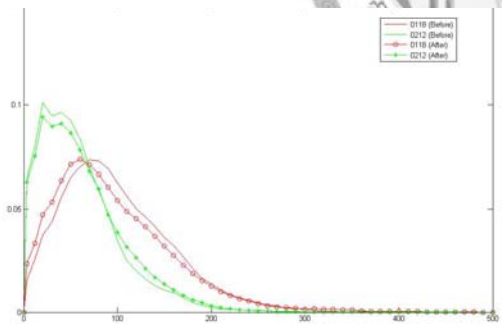

K^{trans}

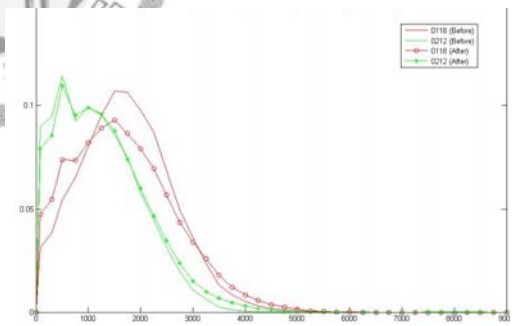

K_{ep}

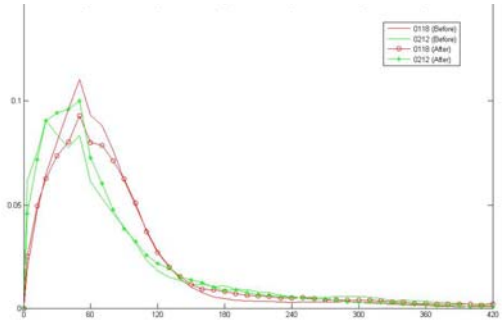

V_e

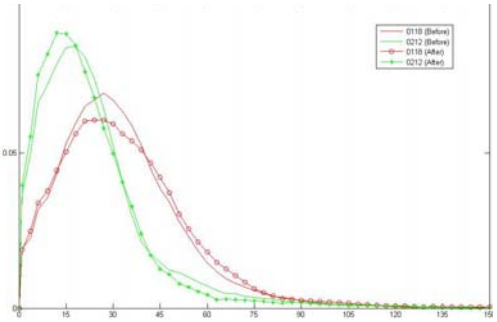

V_p

Group B (F779)

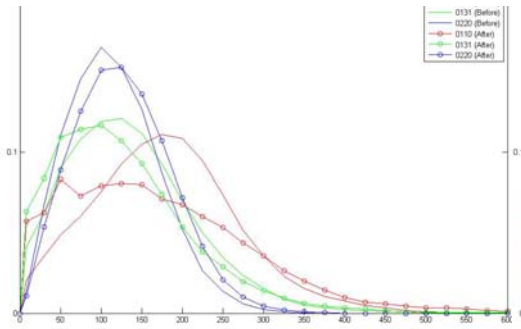

K^{trans}

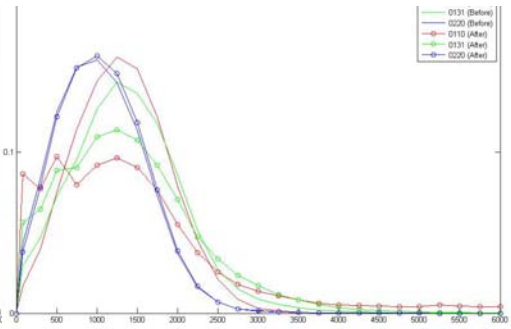

K_{ep}

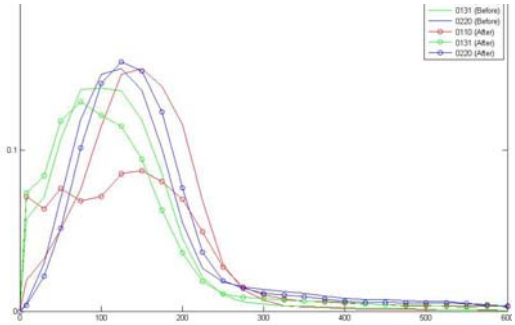

V_e

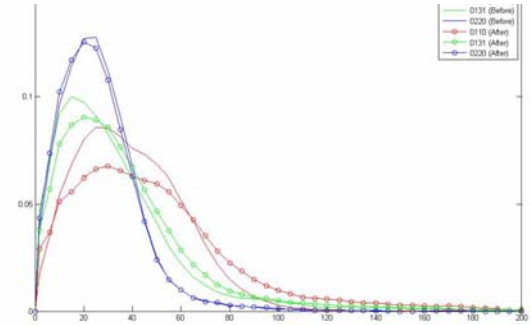

V_p

Group B (M469)

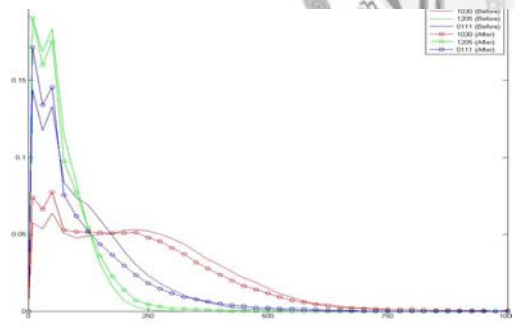

K^{trans}

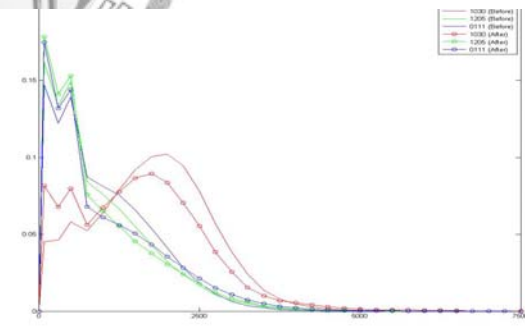

K_{ep}

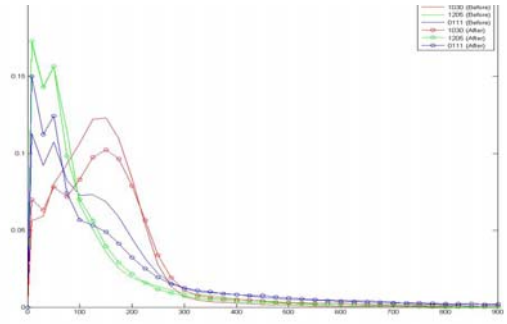

V_e

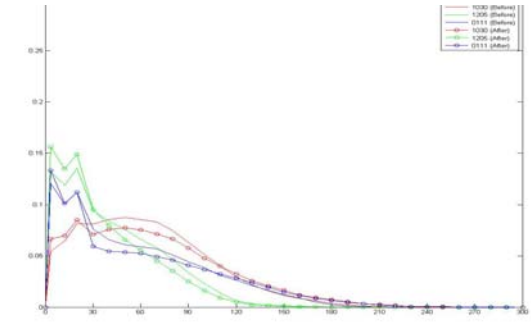

V_p

Group B (M826)

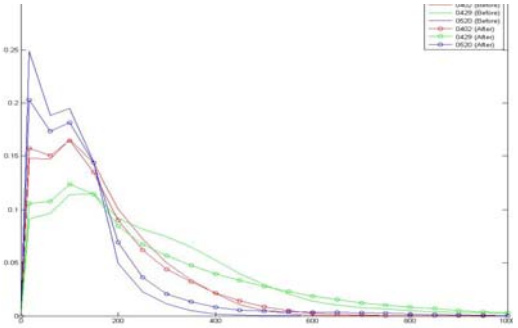

K^{trans}

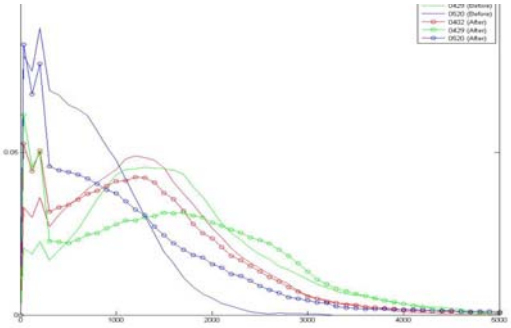

K_{ep}

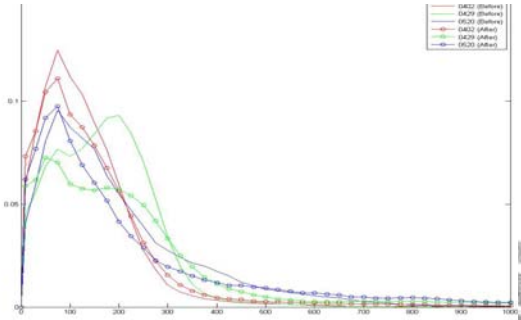

V_e

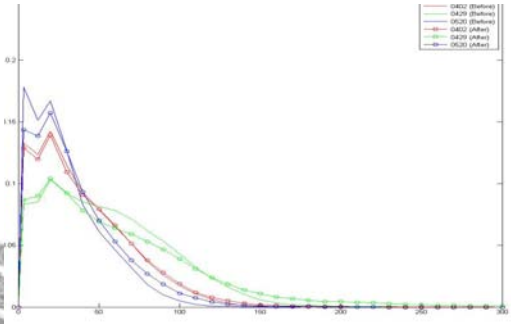

V_p

Group B (M141)

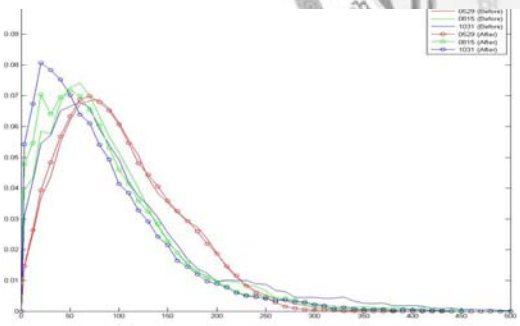

K^{trans}

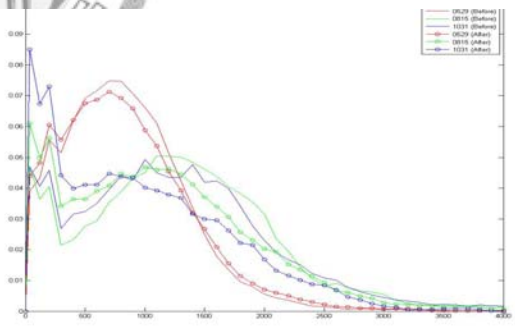

K_{ep}

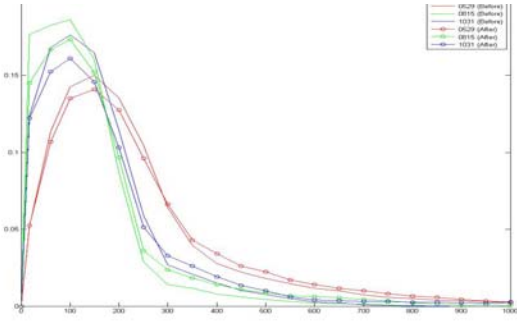

V_e

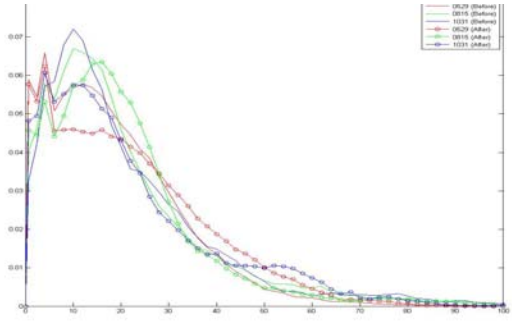

V_p

Group B (F928)

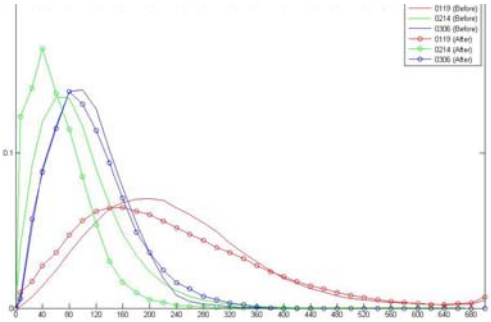

K^{trans}

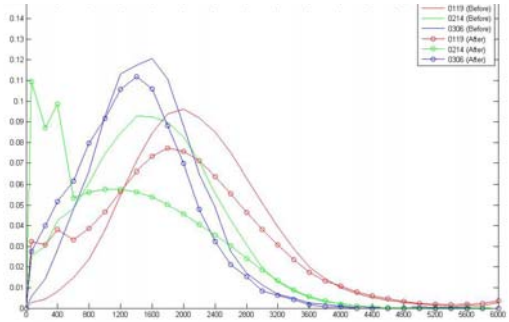

K_{ep}

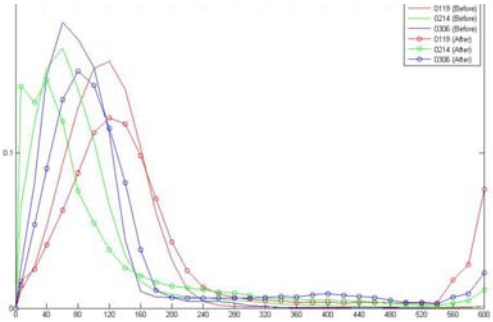

V_e

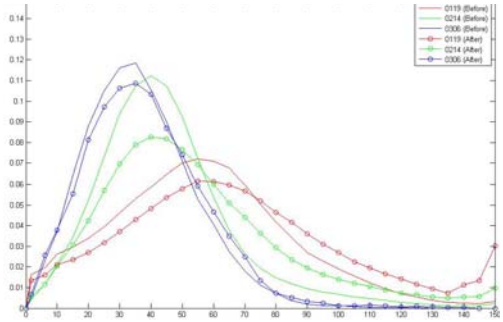

V_p

Group B (M740)

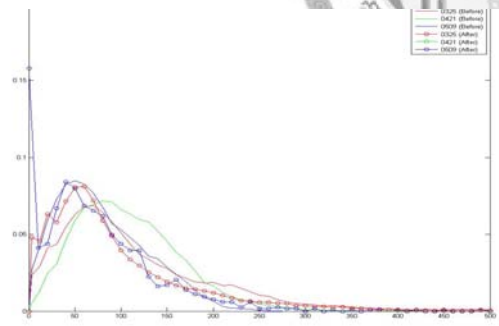

K^{trans}

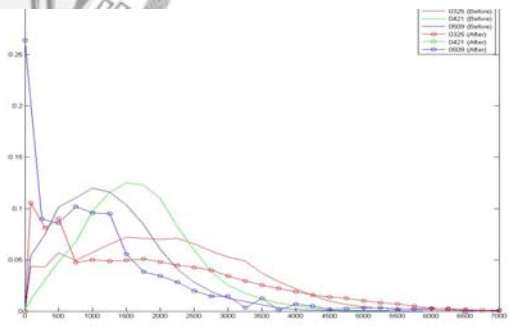

K_{ep}

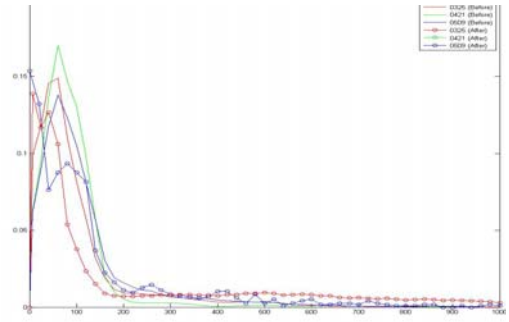

V_e

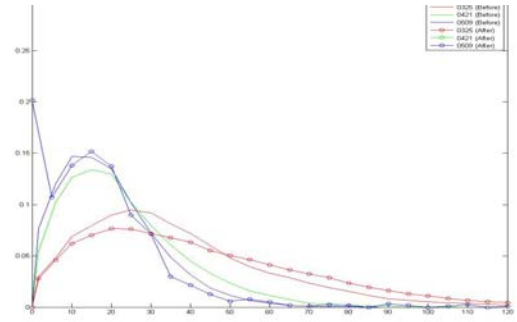

V_p

Chapter 5 Discussion

5.1 Problems in Data Analysis

According to the results present in 4.2, we find almost every patient in group A shows the reasonable results in the figure about four different parameter. The curve after motion correction process will lower and have trend through the vertical axis.

In group B, it also exist the same phenomenon in the distribution curve. But in some patient, the baseline curve (red curve) is in the right side, some final curve (blue curve) is in the middle, and the immediate curve (green curve)is in the left. These kind of data need to be analysis more detail or analysis in another way to explain it.

Besides the curve position will differ (red, green, blue) in each chemotherapy process (Baseline, Immediate, Final), the height in each curve is also different. That's because the area under distribution curve have been normalized to be one. And we can find that in most patients, the baseline curve is the lowest while the final curve is the most height in the diagram.

5.2 Inaccuracy Problems

There may exist some reason to explain the results (from parameter maps) which is not totally satisfy with the situation. First, in our assumption, the tumor shape is solid and stable (not change with time). But in fact, many tumor's shape do have some different. Even in the scan processing, the slice will not so exact to cut, so the image in the same position will differ with each other.

Second, the motion in the lung is in 3 dimensions. It's reasonable to find out the tumor movement in the lung is 3 dimensions, too. Third possible reason is when we select the ROI (Region of Interest), besides the contrast agent area (usually with colorful in parameters map), there also exit a part of the dark side. In other words, the tumor characteristic is not homogeneous in the ROI.

After the motion correction, if the portion of the dark side is increase, although the region we select is more accuracy but the parameters values will change in a worst way. Due to the above possible thing, we should check the motion in tumor itself and the homogeneous problems.

Chapter 6 Conclusion

6.1 Conclusion

From the figure results in data analysis, we can clear identify the distribution difference in histogram between the motion correct process or not. Most of the cases show that after the motion correct, the peak is slower than the case without doing the motion correct. Another phenomenon shows after motion correct, the distribution is more smooth than without doing it.

That is, the motion correct processing not only improve the accuracy in the dynamic image sequences, it change the distribution curve in these four parameters (K^{trans},K_{ep}, V_e,V_p). We can easy identify the treatment trend in the distribution curve. The curve will close to the left side (the vertical axis) when the patient taking the chemotherapy. Although some figure shows the immediate after treatment process is more close to the left side, the patient before treatment must in the rigt side far away from the vertical axis.

To sum up, motion correction not only fixing the registration problems in sequential dynamic images, we also find that it affect the parameters in pharmacokinetics mathematical model. For example: the histogram distribution curve. Due to the complexity in chemotherapy treatment, the DCE-MRI provides us another direction to

evaluate how the influence that the drugs take effect.

The standard in tumor treatment is by the RECIST (Response Evaluation Criteria in Solid Tumors) criteria. We should take our results to compare with the RECIST criteria to adjust its correlation to improve the accuracy.

6.2 Future Work

Since the current motion artifact correction need to be modified, we should do: 1. Using non-rigid body registration method to fit the tumor position. 2. Model the motion due to the breathing movement to 3 dimensions motion Correction.

The application in DCE-MRI works very widely in other organ. For example: Tumor in Human Brain, Breast Cancer. It’s reasonable to state the DCE-MRI will do well if there have very little motion artifact. Inevitably, the lung cancer still have more sever motion problem. It’s worth to do more research in solving the problem.

Reference

1. R. Strecker1, K. Scheffler. DCE-MRI in clinical trials: data acquisition techniques and analysis methods. International Journal of Clinical Pharmacology and Therapeutics 2003;41(12):603–605.

2. A. Jackson, D. L. Buckley. Dynamic Contrast-Enhanced Magnetic Resonance Imaging in Oncology. Springer 2005.

3. http://www.cancer.gov/cancertopics/understandingcancer/angiogenesis/Slide3

4. M.L. George, A.S.K.Dzik-Jurasz. Non-invasive methods of assessing angiogenesis and their value in predicting response to treatment in colorectal Cancer. British Journal of Surgery 2001;88:1628–1636.

5. K.L.Verstraete, J.L. Bloem. Dynamic Contrast-Enhanced Magnetic Resonance Imaging. Springer Berlin Heidelberg 2006;3 rd.

6. Rujirutana Srikanchana, David Thomasson. A Comparison of Pharmacokinetic Models of Dynamic Contrast Enhanced MRI. Proceedings of the 17th IEEE Symposium on Computer-Based Medical Systems (CBMS'04)

7. C .Patlak, R. Blasberg, J. Fenstermacher. Graphical Evaluation of blood-to-brain Barrier transfer constants from multiple time uptake data. J. Cereb. Blood Flow Metab 1983;3:1–7.

8. G. Brix, W. Semmler, R. Port, L. Schad, G. Layer, W. Lorenz. Pharmacokinetic parameters in CNS Gd-DTPA enhanced MR Imaging. J Comput Assist Tomogr 1991; 15:621–628.

9. P. S. Tofts, A. G. Kermode. Measurement of Blood-Brain Barrier Permeability and Leakage Space Using Dynamic MR Imaging. Magnetic Resonance in Medicine 1991;17:357–367.

10. P. S. Tofts, G. Brix, D. L. Buckley. Estimating Kinetic Parameters From Dynamic Contrast-Enhanced T1-Weight MRI of a Diffusable Tracer: Standardized Quantities and Symbols. J.Magn Reson Imaging 1999;10:223–232.

11. H. J. Weinmann, M. Laniado , Phys.Chem.Phys. Med. NMR 1984;16:167.

12. Tofts PS. Modeling tracer kinetics in dynamic Gd-DTPA MR imaging. J Magn Reson Imaging 1997;7:91–101.

13. Nola Hylton. Dynamic Contrast-Enhanced Magnetic Resonance Imaging As an Imaging Biomarker. Journal of clinical oncology 2006;24:20.

14. B Morgan,1, JF Utting2, A Higginson. A simple, reproducible method for monitoring the treatment of tumor using dynamic contrast-enhanced MR imaging. British Journal of Cancer 2006;94:1420–1427

15. David J. Collins, Anwar R. Padhani. Dynamic Magnetic Resonance Imaging of Tumor Perfusion. IEEE Engineering in medicine and biology magazine 2004.

16. Fisher B, Bryant J, Wolmark N. Effect of preoperative chemotherapy on the Outcome of women with operable breast cancer. Journal of Clinical Oncol 1998;16:2672–2685.

17. Makris A, Powles TJ, Ashley SE. A reduction in the requirements for mastectomy in a randomized trial of neo-adjuvant chemo-endocrine therapy in primary breast cancer. Ann Oncol 1998;9:1179–1184.

18. Machiavelli MR, Romero AO, Perez JE. Prognostic significance of pathological Response of primary tumor and metastatic axillary lymph nodes after neoadjuvant Chemotherapy for locally advanced breast carcinoma. Cancer Journal of Society 1998;4:125–131.

19. Chollet P, Amat S, Cure H. Prognostic significance of a complete pathological Response after induction chemotherapy in operable breast cancer. Br J Cancer 2002;86: 1041–1046.

20. Heys SD, Eremin JM. Role of multimodality therapy in the management of locally advanced carcinoma of the breast. Jounnal of Am Coll Surg 1994;179:493–504.

21. Anwar R. Padhani. Prediction of Clinicopathologic Response of Breast Cancer to Primary Chemotherapy at Contrast-enhanced MR Imaging: Initial Clinical Results.Radiology 2006;239: Number 2.

22. Linda G. Shapiro, George C. Stockman. Computer Vision. New Jersey, Prentice-Hall 2001:279–325

23. Jianbo Shi ,Jitendra Malik. Normalized Cuts and Image Segmentation. IEEE Transactions on pattern analysis and machine intelligence 2000;22(8).

24. Z. Wu R. Leahy. An Optimal Graph Theoretic Approach to Data Clustering: Theory and Its Application to Image Segmentation. IEEE Trans. Pattern Analysis and Machine Intelligence 1993;15(11):1,101–1,113.

25. M. Kass, A. Witkin, and D. Terzopoulos. Snakes: Active contour models. Int. J. Comput. Vis. 1987;1:321–331.

26. D. Terzopoulos and K. Fleischer. Deformable models.Vis. Comput. 1988;4:306–331.

27. T. McInerney and D. Terzopoulos. A dynamic finite element surface model for segmentation and tracking in multidimensional medical images with application to cardiac 4D image analysis. Comput. Med. Imag. Graph.1995;19:69–83.

28. F. Leymarie and M. D. Levine. Tracking deformable objects in the plane using an active contour model. IEEE Trans. Pattern Anal. Machine Intell.1993;15:617–634.

29. R. Durikovic, K. Kaneda, and H. Yamashita. Dynamic contour: A texture approach and contour operations. Vis. Comput.1995;11:277–289.

30. B. K. P. Horn and B. G. Schunck. Determining optical flow. Artif. Intell. 1981; 17: 185–203.

31. S. N. Gupta and J. L. Prince. Stochastic models for DIV-CURL optical flow Methods. IEEE Signal Processing Lett.1996;3:32–35.

32. R.Courant and D. Hilbert, Methods of Mathematical Physics. New York: Interscience.1953.

33. Chenyang Xu, Jerry L. Prince. Snakes, Shapes, and Gradient Vector Flow. IEEE Transactions on image processing 1998;7(3).